Targeting OCA-B/Pou2af1 blocks activated, autoreactive T cells in the pancreas and type-1 diabetes

Heejoo Kim[1,2,#], Jelena Perovanovic[1,2], Arvind Shakya[1,$], Zuolian Shen[1,2], Cody N. German[1], Andrea Ibarra[1,2], Jillian L. Jafek[1,2], Nai-Pin Lin[3], Brian D. Evavold[1], Danny H.-C. Chou[3,¶], Peter E. Jensen[1], Xiao He[1], and Dean Tantin[1,2]

[1]Department of Pathology, University of Utah School of Medicine, Salt Lake City, UT 84112, U.S.A.
[2]Huntsman Cancer Institute, University of Utah School of Medicine, Salt Lake City, UT 84112, U.S.A.
[3]Department of Biochemistry, University of Utah School of Medicine, Salt Lake City, UT 84112, U.S.A.

[#]Current address: Johnson & Johnson Research and Development, San Diego, CA 92121
[$]Current address: Bristol Myers Squibb, San Diego, CA 92121
[¶]Current address: Department of Pediatrics, Division of Endocrinology and Diabetes, Stanford University School of Medicine, Palo Alto, CA 94305

Correspondence to: Dean Tantin: dean.tantin@path.utah.edu

Summary: Kim et al. show that loss or inhibition of OCA-B in T cells protects mice from type-1 diabetes.

Running title: OCA-B in T1D

Manuscript data:

Characters in title (including spaces): 94

Words in abstract: 153

Characters (not including spaces, methods, or references): 36,718

Abstract

The transcriptional coregulator OCA-B promotes expression of T cell target genes in cases of repeated antigen exposure, a necessary feature of autoimmunity. We hypothesized that T cell-specific OCA-B deletion and pharmacologic OCA-B inhibition would protect mice from autoimmune diabetes. We developed an *Ocab* conditional allele and backcrossed it onto a diabetes-prone NOD/ShiLtJ strain background. T cell-specific OCA-B loss protected mice from spontaneous disease. Protection was associated with large reductions in islet CD8$^+$ T cell receptor specificities associated with diabetes pathogenesis. CD4$^+$ clones associated with diabetes were present, but associated with anergic phenotypes. The protective effect of OCA-B loss was recapitulated using autoantigen-specific NY8.3 mice, but diminished in monoclonal models specific to artificial or neoantigens. Rationally-designed membrane-penetrating OCA-B peptide inhibitors normalized glucose levels, and reduced T cell infiltration and proinflammatory cytokine expression in newly-diabetic NOD mice. Together, the results indicate that OCA-B is a potent autoimmune regulator and a promising target for pharmacologic inhibition.

Keywords

OCA-B, *Pou2af1*, Type-1 Diabetes, T lymphocytes, single-cell RNAseq

Introduction

Type 1 Diabetes (T1D) is an autoimmune disease in which the host immune system is directed towards antigens associated with pancreatic beta cells (Cooke and Plotnick, 2008; Lernmark and Larsson, 2013). Pathologically, T1D is characterized by insulitis, beta cell destruction and inability to produce insulin. The main treatment for T1D, life-long insulin therapy, treats symptoms but not cause. The development of new T1D treatments is limited by an incomplete understanding of disease mechanisms (Staeva et al., 2013). Beta cell regeneration is a promising line of therapy, but still requires methods to specifically block T1D autoimmunity. An ideal therapy would block autoimmunity early in the disease course to spare remaining beta cell function while preserving normal immune function.

OCA-B, also known as Bob.1/OBF-1 (gene symbol *Pou2af1*), is a transcriptional coregulatory protein named for its strong expression in the B cell lineage, where it is dispensable until after B cell activation. Following B cell activation, it is essential for the generation of germinal centers (Shi et al., 2015). In $CD4^+$ T cells, OCA-B docks with the transcription factor Oct1 to regulate a set of ~150 target genes, including *Il2*, *Ifng* and *Csf2* (*Gmcsf*) (Shakya et al., 2015). Upon T cell activation, many of these targets are activated by pathways that converge on transcription factors such as NF-AT, AP-1 and NF-κB. Factors like NF-AT can be thought of as the primary on/off switches for these genes, and drugs that block their activity effectively block target gene expression. Such drugs have utility in many contexts, but also have drawbacks including global dampening of immune function and side effects due to expression in other tissues. In contrast, Oct1 and OCA-B insulate silent but previously activated target genes against stable repression. Loss of either protein does not affect $CD4^+$ T cell responses to stimulation in vitro or primary infection in mice (Kim et al., 2019; Shakya et al., 2015), but causes target gene expression defects upon secondary stimulation in vitro (Shakya et al., 2015; Shakya et al., 2011). Loss of either protein also results in defective $CD4^+$ memory T cell formation and recall responses in vivo (Shakya et al., 2015). In addition, OCA-B expression is largely confined to lymphocytes. OCA-B is undetectable in thymocytes and naïve $CD4^+$ T cells, but becomes stably expressed after antigen stimulation (Shakya et al., 2015). Once expressed, OCA-B recruits the histone lysine demethylase Jmjd1a/Jhdm2a/Kdm3a to Oct1 at target loci, where it locally removes inhibitory H3K9me2 chromatin marks that would otherwise promote repressive chromatin environments (Shakya et al., 2015). OCA-B also potentiates polarization of activated helper T cells towards the Th17 phenotype, among the most pro-inflammatory helper T cell subsets (Yosef et al., 2013).

Persistent antigen exposure is a common property of autoimmune responses. Among profiled $CD4^+$ T cell subsets, OCA-B levels are elevated in both central memory cells and pancreas-infiltrating,

83 islet-reactive CD4$^+$ T cells (Heng et al., 2008). Both Oct1 and OCA-B are highly conserved from mice
84 to humans, and genome-wide association studies identify Oct1/OCA-B binding site polymorphisms
85 that confer predisposition to a variety of human autoimmune diseases including T1D, multiple
86 sclerosis, lupus, inflammatory bowel disease and rheumatoid arthritis (Cunninghame Graham et al.,
87 2006; Farh et al., 2015; Kiesler et al., 2009; Leon Rodriguez et al., 2016; Maurano et al., 2012; van
88 Heel et al., 2002; Vince et al., 2016). Other studies implicate polymorphisms at the *Ocab* (*Pou2af1*)
89 locus itself in different forms of autoimmunity (Games Collaborative et al., 2006; Nakamura et al.,
90 2012). We therefore hypothesized that targeting OCA-B would inhibit autoreactive, diabetogenic T
91 cell responses.
92 Here, we generate a T cell conditional mouse model of OCA-B deficiency. We show that
93 OCA-B ablation protects animals from spontaneous, polyclonal T1D. Protection was associated with
94 reduced autoantigen-specific CD8$^+$ TCR clones in the pancreatic islets, and the induction of anergy in
95 potentially autoreactive CD4$^+$ T cell clones. The protection associated with OCA-B loss varied among
96 different TCR transgenic and monoclonal antigen models, and was weakest using synthetic antigens
97 and monoclonal transplant models. Protection was stronger using a spontaneous autoantigen-specific
98 TCR transgenic model. Using a rational-design approach, we developed membrane-penetrating OCA-
99 B peptide inhibitors that are efficacious in vitro and in mice. Collectively, the results show that OCA-B
100 is a potent and pharmacologically accessible autoimmune regulator.

101 **Results**

102 **Generation of an *Ocab* conditional allele and NOD backcrossing**

103 We generated a conditional *Ocab* (*Pou2af1*) mouse allele using embryonic stem cells provided by the
104 knockout mouse project (KOMP) repository. Deletion of the *LoxP* sites creates a null allele by
105 removing the first three exons (Fig. S1A). Breeding chimeric mice resulted in germline transmission
106 and a founder mouse (Fig. S1B, lane 2) that was crossed to a FLP deleter mouse strain (FLP^{Rosa26}) to
107 remove the reporter cassette and create a floxed conditional allele (Fig. S1A and B, lane 3).
108 Intercrossing these mice generated *fl/fl* homozygotes (Fig. S1B, lane 4) which were crossed to a
109 germline Cre deleter strain (Cre^{Rosa26}) to generate germline null (*Δ*) alleles (lanes 5 and 6). As
110 expected, homozygous *fl/fl* mice produce normal amounts of both p34 and p35 OCA-B protein
111 isoforms (Fig. S1C, lane 6), while no protein of either isoform is present in *Δ/Δ* spleens (lanes 7-8).
112 These results indicate that the *fl* allele is OCA-B sufficient and the Cre-deleted allele is a null. Crossing
113 the *fl* allele onto a CD4-cre driver, which deletes in both CD4 and CD8 compartments, resulted in
114 efficient deletion in splenic T cells (Fig. S1D). This allele therefore represents a robust system in
115 which to study OCA-B function in T cells.

116 The conditional allele was generated on a C57BL/6 background. To test the role of OCA-B
117 expression in T cells in T1D emergence, we conducted congenic backcrosses to the NOD strain
118 background. This method allows spontaneous diabetes to be produced rapidly by screening and
119 selectively breeding mice with 13 microsatellite and SNP markers associated with autoimmunity
120 (Serreze et al., 1996). *Ocab* is located on mouse chromosome 9 and distant from any of the *Idd* loci.
121 Following these markers with specific primer-pairs (Table S1), we produced backcrossed animals with
122 all 13 markers (Fig. S1E) that recapitulate spontaneous autoimmunity (not shown). For example, *Idd1*,
123 which maps to the MHC region (Hattori et al., 1986), converted to the homozygous NOD allele after 2
124 backcross generations (Fig. S1E, lane 3), whereas *Idd13*, which maps near beta-2-microglobulin
125 (Serreze et al., 1998) became NOD homozygous after 4 generations (lane 4). Genotyping identified
126 this fourth-generation backcrossed animal as having all 13 microsatellite markers and the *Ocab*
127 conditional allele (Fig. S1F, #122). This founder animal was crossed to NOD.CD4-cre in order to
128 delete OCA-B in T cells. Similar NOD backcrosses, conducted using *Ocab* null mice (Kim et al.,
129 1996), resulted in OCA-B germline-deficient NOD mice (not shown). As with the original C57BL/6
130 OCA-B germline knockout (Kim et al., 1996), all alleles were viable and fertile with no obvious health
131 issues.

132

133 **Normal baseline T cell Status in NOD mice lacking OCA-B**

134 To study the effects of T cell-specific OCA-B loss on T cell function, we performed single-cell RNA
135 sequencing (scRNAseq) and TCR clonotype analysis using $CD3^+$ T cells isolated from PLNs of
136 prediabetic 8 wk-old female NOD.*Ocab*$^{fl/fl}$CD4-cre or NOD.*Ocab*$^{fl/fl}$ littermate controls. For each
137 group, cells from 3 animals were combined for microfluidics, sequencing and analysis. ~6000
138 knockout and ~3000 control cells were identified in this analysis, most of which comprise naïve $CD4^+$
139 and $CD8^+$ cells (Fig. S2A, pink and orange), and regulatory T cells (Tregs, green). There was also a
140 small population of activated $CD4^+$+$CD8^+$ cells (blue-green), presumably in the process of exiting the
141 lymph nodes. Other than a small decrease in the percentage of activated T cells (4.4 vs 6.1%), few
142 differences in relative abundance of the populations were observed. None of the populations expressed
143 measurable amounts of *Ocab* (*Pou2af1*) mRNA (not shown), however *Pou2af1* is expressed at low
144 levels in T cells making it difficult capture by scRNAseq. In addition, few changes in gene expression
145 were identified (Fig. S2B, Table S2). We also determined TCR repertoires, identifying few changes
146 across all populations (Fig. S2C). However, specific sub-populations did show changes in TCR
147 utilization. For example, >90% of NOD $CD8^+$ T cells that display reactivity to islet-specific glucose-6-
148 phosphatase catalytic subunit related protein (IGRP) residues 206-214 express *Trbv13-3* (Vβ8.1)
149 (Wong et al., 2006). Although this clone was unchanged across the entire population of T cells (Fig.
150 S2C), it was over-represented in the effector $CD8^+$ population (Fig. S2D). In contrast, other TCR
151 clonotypes such as *Trbv13-1*, *Trbv13-2*, *Trbv1* and *Trbv15* were unchanged (not shown).

152

153 **NOD mice lacking OCA-B are protected from T1D**

154 T1D onset in NOD mice is spontaneous and acute (Makino et al., 1985). To test the impact of OCA-B
155 loss in T cells on spontaneous T1D, we compared incidence in in female NOD.*Ocab*$^{fl/fl}$CD4-cre mice,
156 and littermate controls lacking CD4-cre. Glucose was monitored 2-3 times/wk. Approximately 60% of
157 *Ocab*$^{fl/fl}$ control mice manifested spontaneous diabetes by 24 weeks of age, reaching an average of
158 >300 mg/dL by 24 weeks, while no *Ocab*$^{fl/fl}$CD4-cre mice became diabetic (Fig. 1A,B). Similar results
159 were observed using female whole-body knockout NOD.*Ocab*$^{-/-}$ compared to *Ocab*$^{+/+}$ littermate
160 controls. While ~80% of control females developed T1D within 24 weeks after birth, only ~20% of
161 NOD.*Ocab*$^{\Delta/\Delta}$ females did so (Fig. 1C). The differences in T1D penetration are likely attributable to
162 differences in the NOD backcrosses, as the 13 *Idd* NOD determinants largely but not completely
163 dictate the autoimmune phenotype. Cumulatively, the results show that OCA-B expression in T cells is
164 critical for T1D pathogenesis in NOD mice.

165 We sacrificed *Ocab*$^{fl/fl}$CD4-cre female mice and controls at 24 weeks, and determined immune
166 cell frequencies in the pancreata. We observed more T cells in the pancreata of OCA-B deficient mice
167 (not shown). An relative increase in infiltrating T cells in endpoint knockouts at endpoint is
168 understandable because the controls have annihilated their pool of beta cells and associated antigens.
169 We also studied pancreatic macrophages in these mice. Islet infiltration of F4/80^{+}CD11b^{+} macrophages
170 is critical for NOD T1D pathogenesis both in spontaneous and adoptive transfer T1D models (Peterson
171 et al., 1998; Rosmalen et al., 2000). CCL1 expressed in diabetogenic CD4^{+} T cells recruits CCR8-
172 expressing macrophages (Cantor and Haskins, 2007). OCA-B deletion decreases *Ccl1* mRNA
173 expression in stimulated, rested and re-stimulated CD4^{+} T cells compared to controls (Table S3).
174 Despite the presence of antigen greater numbers of T cells, we observed fewer macrophages in 24 wk
175 NOD.*Ocab*$^{fl/fl}$CD4-cre islets (Fig. 1D,E). In contrast, macrophages were unaffected by T cell-specific
176 OCA-B loss in prediabetic (8 wk) mice (Fig. 1D).
177 IFNγ is a direct OCA-B target gene (Shakya et al., 2015). Serum and pancreatic IFNγ levels
178 gradually rise in young NOD mice, reaching maximum at diabetes onset (Schloot et al., 2002).
179 Diabetogenic CD4^{+} and CD8^{+} T cells express IFNγ both in humans and NOD mice (Krishnamurthy et
180 al., 2008; Newby et al., 2017; Wang et al., 1997). We therefore predicted that OCA-B loss would
181 reduce IFNγ expression in islet CD4^{+} and CD8^{+} T cells. We compared IFNγ-expressing pancreatic
182 CD4^{+} and CD8^{+} T cells in female NOD.*Ocab*$^{fl/fl}$CD4-cre to littermate control mice lacking CD4-cre. In
183 12 wk prediabetic mice, CD8^{+} T cell frequencies were only slightly decreased (Fig. 1F). CD4^{+} T cells
184 at the same timepoint were also unchanged (not shown). At the time of diabetes onset (16 wk), fewer
185 IFNγ-expressing CD8^{+} T cells were present in *Ocab* conditional-deleted mice compared to controls
186 (Fig. 1G).
187
188 **T cell-specific OCA-B deletion alters the islet-infiltrating TCR repertoire**
189 We performed scRNAseq and TCR clonotype analysis similar to Fig. S2, but using older (12 wk)
190 prediabetic NOD.*Ocab*$^{fl/fl}$CD4-cre or NOD.*Ocab*$^{fl/fl}$ littermate control female mice, and using total
191 CD45^{+} cells isolated from pancreatic islets. Cells were isolated from 4 animals/group and combined for
192 microfluidics and sequencing. After filtering, ~6200 knockout and ~3800 control cells were identified.
193 Overlaying cells from both genotypes, we used their gene expression profiles to definitively identify
194 cell lineages, including naïve T cells, memory/effector CD4^{+} T cells, memory/effector CD8^{+} T cells, B
195 cells, macrophages and neutrophils (Fig. 2A). Among the different populations, the biggest relative
196 change was neutrophils, which decreased from 3.4 to 1.4% in conditional knockout islets (Fig. 2A). B

197 cells were also decreased, albeit more slightly. These changes were accompanied by increased
198 percentages of naïve T cells (32 vs. 25%). Prediabetic islets also showed significant changes in gene
199 expression between the 2 groups (Fig. 2B), the strongest of which occurred in neutrophils (e.g., *Cxcl2*,
200 down), memory/effector $CD8^+$ T cells (*Ccl4*, *Tcrg-v1*, *Itga*, down; *Tcrbv1*, *Trav8n-2*, up), NK T cells
201 (*Klra2*, *Lars2*, down) and γδT cells (*Gzma*, *Gzmb*, *Ccl5*, down).
202 We also profiled TCR utilization in pancreatic T cells. Across total T cells, few changes were
203 observed (Fig. S3), however this was largely do to similar representation in the naïve T cell pool.
204 Isolating antigen-experienced $CD4^+$ and $CD8^+$ effector + memory subpopulations revealed sharp
205 differences. For example, >90% of diabetogenic $CD8^+$ T cells displaying reactivity to $IGRP_{206-214}$
206 express *Trbv13-3* (Vβ8.1) (Wong et al., 2006). Relative to controls, this clonotype was under-
207 represented in OCA-B deficient effector + memory $CD8^+$ cells (Fig. 2C, 20.9% vs 8.6%). Based on
208 this information, we repeated the clonotype analysis, but only using the effector + memory $CD8^+$ T cell
209 cluster. Within this population, dominant TCR clonotypes were strikingly different (Fig. 2D).
210 Clonotype 1 for example is the most abundant, and corresponds to a TCRα V8N-2 chain paired with
211 TCRβ V1 or V15. It has not been associated with T1D. This clonotype was absent in control islets but
212 represented >4% of OCA-B deficient islet $CD8^+$ effector + memory T cells (Fig. 2D). Clonotype 1
213 cells overlaid with both genotypes is shown in Fig. 2E. Clonotype 2 by contrast expresses the T1D-
214 associated Vβ8.1 TCR β chain. This clonotype was strongly represented in controls (>3%) but absent
215 from OCA-B deficient effector + memory $CD8^+$ cells (Fig. 2D). In contrast to CD8, CD4-dominant
216 TCR clonotypes associated with T1D were still present in knockouts, but associated with markers of
217 anergy. For example, clonotype 4 (*Trav13-1/16N+Trbv15*) is associated with pro-diabetogenic, BDC-
218 reactive $CD4^+$ T cells (Li et al., 2009). This clonotype was enriched in the OCA-B deficient effector +
219 memory $CD4^+$ cells, but only in a CTLA4- and FR4-expressing sub-population (Fig. 2E).
220 Cumulatively, these results show that OCA-B loss from T cells significantly skews the TCR landscape
221 of islet effector/memory-like T cells to an anti-diabetogenic phenotype.
222

223 **Autoantigen-specific CD8+ T cells are present in PLNs of OCA-B deficient mice, but show**
224 **reduced reactivity and islet penetration**

225 In order to understand the basis for the reduction in autoantigen-specific $CD8^+$ T cell islet clones, we
226 studied Vβ8.1 expression and $IGRP_{206-214}$ reactivity in matched pancreatic islets and PLNs from 12 wk
227 prediabetic female *Ocab*$^{fl/fl}$CD4-cre mice or littermate *Ocab*$^{fl/fl}$ controls. Islet $CD8^+$ T cells showed
228 decreased Vβ8.1 usage (Fig. 3A), while PLNs from the same animals showed a corresponding increase

229 (Fig. 3B). To directly test diabetogenic, antigen-specific islet $CD8^+$ T cells, we used $IGRP_{206-214}$ H-$2K^d$
230 class I tetramers, which recognize TCRs expressing Vβ8.1. Islet $CD8^+V\beta8.1^+$ T cells showed a strong
231 decrease in $IGRP_{206-214}$ specificity (Fig. 3C).
232 The decrease in autoantigen-specific islet $CD8^+$ T cells and corresponding increase in the PLNs
233 in OCA-B T cell deficient mice raised two possibilities: cells in the PLNs could fail to become
234 activated, or could become activated but fail to migrate to the pancreas. In the first case, more antigen-
235 reactive cells would be observed while in the second there would be fewer. To distinguish between
236 these possibilities, we performed peptide stimulation experiments using 7 different known
237 diabetogenic self-peptides. We used 5 IGRP peptides, including $IGRP_{206-214}$ which corresponds to the
238 tetramer used above and the NY8.3 TCR transgenic mice used below. We also used two GAD65
239 epitopes, 206-214 and 546-554. 5 of the 7 peptides showed significant reductions in autoreactivity,
240 including $IGRP_{206-214}$ (Fig. 3D,E). These results indicate that potentially autoreactive cells fail to
241 become activated in the PLNs of OCA-B deficient mice.
242
243 **Protection conferred by OCA-B loss is model-specific**
244 T1D in NOD mice originates from defective negative selection in developing T cells, resulting in T
245 cell autoreactivity. OCA-B is not expressed in thymocytes and OCA-B loss does not appear to affect T
246 cell development (Shakya et al., 2015). Therefore, the protective effect of OCA-B loss in T cells likely
247 arises from blunting pre-existing autoreactivity in the periphery. To test the hypothesis that OCA-B
248 loss confers protection in simplified systems, we crossed OCA-B deficient mouse models employing
249 TCR transgenes and model antigens.
250 We crossed the germline null *Ocab* allele to BDC2.5 mice (Katz et al., 1993), which expresses
251 a CD4-restricted TCR specific for a hybrid insulin-chromogranin A peptide (Delong et al., 2016).
252 Transferring Treg-depleted T cells from BDC2.5 TCR transgenic mice into NOD.Scid mice results in
253 disease after approximately 10 d (Berry and Waldner, 2013; Presa et al., 2015). We transferred
254 $CD4^+CD25^-$ T cells from germline $Ocab^{-/-}$ or $Ocab^{+/+}$ BDC2.5 mice into NOD.Scid recipients,
255 monitoring diabetes emergence. Transplants from both $Ocab^{-/-}$ and control NOD.BDC2.5 mice resulted
256 in equivalent disease kinetics (Fig. 4A) and severity (not shown). Transferring $Ocab^{-/-}$ or control
257 NOD.BDC2.5 $CD4^+CD62L^+V\beta4^+$ T cells into NOD.Scid recipients, or total $CD4^+$ T cells into NCG
258 recipients, also resulted in equivalent disease (Fig. S4A, Fig. 4B).
259 We also tested the effect of T cell conditional OCA-B deletion in a different strain background,
260 C57BL/6J, using the artificial membranous chicken ovalbumin antigen expressed from the rat insulin

261 promoter (RIP-mOVA) (Van Belle et al., 2009). Wild-type OVA-reactive $CD8^+$ OT-I T cells were
262 transferred into either *Ocab*$^{fl/fl}$CD4-cre or control *Ocab*$^{fl/fl}$ RIP-mOVA mice. In this model, host $CD4^+$
263 T cells help transferred OT-I T cells promote T1D pathogenesis (Kurts et al., 1997). Mice were
264 infected with Lm-OVA to induce strong and synchronous beta cell destruction and loss of glucose
265 control (>400 mg/dL). No differences were observed using host mice with or without OCA-B T cell
266 deletion (Fig. S4B). These results indicate that OCA-B does not act analogously to transcription factors
267 that regulate many of the same genes, such as NF-AT. Knockouts of these factors would result in
268 broad immunosuppression and protection from T1D across models. Rather, our results suggest that
269 OCA-B loss selectively blunts immune activation in contexts such as autoantigen recognition. To test
270 this supposition and rule out the possibility that T cell transfer itself does not blunt the effect of OCA-
271 B loss, we transferred total splenocytes from polyclonal NOD.*Ocab*$^{fl/fl}$CD4-cre mice or controls. This
272 model, which takes weeks rather than days to develop T1D, recapitulates robust T1D protection with T
273 cell-specific OCA-B loss (Fig. 4C). Protection was associated with fewer IFNγ-expressing islet
274 cytotoxic T cells (Fig. 4D), and reduced insulitis in pancreatic histological sections (Fig. 4E,F).
275 Because the Vβ8.1 clonotype and $IGRP_{206-214}$-reactive cells were significantly attenuated in the
276 islets of T cell conditional OCA-B deficient mice (Fig. 2C-E, Fig. 3A-C), we crossed the *Ocab*
277 germline allele to the NY8.3 TCR transgenic line, which expresses a CD8-restricted TCR directed
278 towards $IGRP_{206-214}$ and manifests spontaneous T1D (Verdaguer et al., 1997). We passively monitored
279 *Ocab*$^{-/-}$ or control *Ocab*$^{+/+}$ NY8.3 mice for T1D development. Significant protection was observed
280 (Fig. 4G, HR=0.4472, p=0.0352), though the degree of protection was less than in OCA-B germline
281 knockout polyclonal models. Together with the decreased IGRP reactivity in OCA-B deficient PLNs,
282 this result indicates that OCA-B promotes T1D in peripheral auto-reactive $CD8^+$ T cells. Using
283 immunoblotting with OCA-B antibodies, we confirmed that OCA-B is expressed in primary splenic
284 C57BL/6 $CD8^+$ T cells. Unlike $CD4^+$ cells where OCA-B is undetectable in naïve cells but becomes
285 induced with prolonged activation (Fig. 4H, top panels), OCA-B^+ could be detected in naïve $CD8^+$
286 cells was rapidly augmented upon activation (Fig. 4H, lanes 1-2). Similar to $CD4^+$ cells, expression
287 was stably maintained when the stimulus was removed and cells were rested with IL-2 (lane 6).
288
289 **OCA-B deficiency promotes $CD4^+$ T cell anergy in vitro**
290 CD8-restricted TCR clones associated with T1D are depleted from the islets of OCA-B T cell
291 conditional mice. In contrast, CD4-restricted clones are increased but associated with an anergic
292 phenotype (Fig. 2E). Anergy is a peripheral tolerance mechanism in which T cells that encounter

293 antigen without co-stimulation become nonfunctional (Kalekar et al., 2016; Kearney et al., 1994;
294 Vanasek et al., 2001). Normal naïve primary $CD4^+$ T cells can be activated in culture by TCR and
295 costimulatory receptor activation, e.g. with anti-CD3ε/CD28 antibodies. Providing TCR signals
296 without CD28 antibodies generates anergic responses (Chai and Lechler, 1997). Interestingly, OCA-B
297 is induced to the same extent with or without co-stimulation (Fig. 5A). To determine if OCA-B loss
298 promotes anergic $CD4^+$ T cell responses, we stimulated naïve splenic $CD4^+$ T cells from germline
299 knockout *Ocab*$^{-/-}$ and control *Ocab*$^{+/+}$ animals ex vivo using plate-bound anti-CD3ε antibodies without
300 co-stimulation, and restimulated the cells with PMA/ionomycin. IL-2 responses were weak in
301 restimulated cells, as expected given the absence of initial costimulation. $CD4^+$ T cells lacking OCA-B
302 generated ~2.5-fold less IL-2 (Fig. 5B,C), indicating that OCA-B provides a barrier against anergic
303 responses.
304 In $CD4^+$ cells, ICOS (Inducible T-cell Costimulator) promotes the induction of T cell anergy
305 (Dong et al., 2001; Dong and Nurieva, 2003; Tuettenberg et al., 2009) and is up-regulated by Oct1 loss
306 in naïve T cells subjected to stimulation under anergic conditions (Kim et al., 2019). Oct1 loss also
307 elevates expression of FR4 and CD73 (Kim et al., 2019) the co-expression of which is a marker for
308 anergy (Kalekar et al., 2016; Martinez et al., 2012). To determine whether OCA-B loss similarly
309 affects expression of these proteins, we stimulated naïve splenic $CD4^+$ T cells
310 ($CD8a^{neg}CD11b^{neg}CD45R^{neg}DX5^{neg}Ter\text{-}119^{neg}CD44^{lo}$) from 6 wk-old *Ocab*$^{fl/fl}$CD4-cre and littermate
311 control CD4-cre male NOD mice for 2 d ex vivo using anti-CD3ε antibodies ± costimulation. Cells
312 were then rested for an additional 2 d. Across all conditions, $CD4^+CD44^+FR4^{hi}CD73^{hi}$ anergic cells
313 were present at >2-fold higher frequency in the OCA-B deficient condition (Fig. 5D). The fraction of
314 $CD44^+$ cells that express ICOS was similarly elevated in cells lacking OCA-B, though only without
315 costimulation (Fig. 5E). Additionally, the expression of the activation marker CD25 was slightly
316 decreased (Fig. 5F). Cumulatively these results suggest that OCA-B loss in $CD4^+$ T cells institutes
317 higher immune thresholds by augmenting anergic responses.
318

319 **Generation of an OCA-B peptide inhibitor**

320 The normal T cell developmental and primary immune response phenotypes observed with OCA-B
321 genetic deletion suggested the possibility of a "therapeutic window" in which targeting OCA-B
322 pharmacologically would blunt autoimmunity while minimally affecting baseline immune function.
323 Based on available OCA-B structural information, we generated a membrane-permeable peptide
324 inhibitor of OCA-B's downstream effector functions. Oct1 interacts with Jmjd1a in a MEK/ERK-

325 dependent manner (Shakya et al., 2015; Shakya et al., 2011) and contains two potential ERK phospho-
326 acceptor serines. The structure of the Oct1 DNA binding domain complexed with consensus octamer
327 binding site DNA (Klemm et al., 1994) reveals that these Oct1 serines are located in the flexible,
328 solvent-exposed linker domain, which connects the two DNA binding sub-domains (Fig. 6A, red
329 dashed line). In contrast with Oct1, OCA-B constitutively interacts with Jmjd1a (Shakya et al., 2015).
330 The OCA-B N-terminus has been solved in complex with the Oct1 DNA binding domain and
331 consensus octamer DNA (Chasman et al., 1999). This region of OCA-B is critical for both Oct1
332 binding and transcription activity (Gstaiger et al., 1996). To identify potential Jmjd1a-interacting
333 OCA-B regions, we aligned the full-length Oct1 and OCA-B amino acid sequences to a cofactor
334 interaction surface of androgen receptor (AR), which also interacts with Jmjd1a (Yamane et al., 2006).
335 Human AR mutations that cause androgen insensitivity have been mapped to residues 698-721 (Thin et
336 al., 2002). Aligning this span to Oct1 identifies the linker domain as the top hit (Fig. 6B). The
337 alignment shows conservation of 3 out of 4 deleterious AR mutations (asterisks). The mutation site that
338 is not conserved is a potential ERK target serine in Oct1, and a phospho-mimetic glutamic acid residue
339 in AR (blue box). These findings suggest that the Oct1 linker domain constitutes a surface which when
340 phosphorylated interacts with Jmjd1a.
341 As with Oct1, alignment with OCA-B identifies a potential Jmjd1a interacting surface (Fig.
342 6B). Unlike Oct1, a glutamic acid residue (Glu30) aligns with AR. Furthermore, the OCA-B residues
343 aligning to AR lie on one side of an alpha-helix (Fig. 6A). Glu30 (red), Leu31 (yellow), Arg34 (blue)
344 and His38 (blue) may therefore constitute a Jmjd1a docking surface. These residues are conserved
345 between mouse and human (Fig. 6C). We mutated OCA-B L31 and R34 to alanine in a transient
346 expression plasmid, and transfected the double-point mutant or parent plasmid control into HCT116
347 cells, which do not express endogenous OCA-B. Control co-IP using Jmjd1a antibodies and lysates
348 from cells expressing wild-type OCA-B confirms the interaction (Fig. 6D, lane 5), while the mutant
349 OCA-B protein failed to interact (lane 8). The mutant was expressed equivalently to WT (lanes 2, 3).
350 These results show the importance of OCA-B residues 30-38 for cofactor interactions.
351 We synthesized three overlapping peptides corresponding to the OCA-B N-terminus (Fig. 6E,
352 peptides #1, #2 (hereafter called "JumOCA") and #3), as C-terminal fusions to the HIV Tat protein for
353 membrane permeability (Schwarze et al., 2000). Initial preparations were conjugated to FITC to enable
354 peptide tracking. Incubating total splenic or pancreatic $CD3^+$ T cells in ex vivo culture with 45 μM Tat-
355 fused JumOCA peptide for 15 min significantly concentrated the peptide within cells. Control OVA-
356 fused peptide lacking membrane-penetrating properties showed no effect (Fig. S5). We then treated
357 splenic $CD4^+$ T cells with the Tat-fused peptides. Prior work has shown that 6 hr restimulation of

358 resting but previously activated OCA-B deficient $CD4^+$ T cells results in decreased expression of target
359 genes such as *Il2* (Shakya et al., 2015). Using this assay with 50 μM JumOCA peptide (every other day
360 with media changes during rest and restimulation) inhibited *Il2* mRNA expression relative to β-actin
361 by ~10-fold (Fig. 6F, compare Tat peptide to JumOCA). Although treated cells showed no obvious
362 changes in viability, morphology or expansion during the course of the assay (not shown), there was a
363 2-3-fold nonspecific diminution of activity associated with unfused Tat peptide (Fig. 6F, compare Tat
364 peptide with no peptide), which has been associated with toxicity (Caron et al., 2004; Krautwald et al.,
365 2004; Polo et al., 2004). Similar results were obtained with the larger peptide #3 but not with peptide
366 #1 (not shown). Peptide #1 is missing residues important for the Jmjd1a interaction based on
367 mutagenesis (Fig. 6B). For all further experiments, we used the JumOCA peptide.
368 We then synthesized a Tat-conjugated peptide using a scrambled JumOCA sequence. This
369 peptide has the same amino acid composition, mass and pI, but should not be able to efficiently
370 compete for Jmjd1a. We used the Tat-only, scrambled and JumOCA peptides with flow cytometry to
371 assess IL-2 production in restimulated $CD4^+$ T cells. JumOCA significantly inhibited IL-2 production
372 relative to the scrambled control, however there were significant toxicities associated with both the
373 scrambled and Tat-only peptides relative to vehicle (Fig. 6G). An example mouse from this experiment
374 is shown in Fig. 6H.
375 The above results are consistent with the JumOCA peptide operating via Jmjd1a competitive
376 inhibition. To test this directly, we used scrambled, double point mutant and wild-type (JumOCA)
377 peptides (lacking the Tat membrane penetrating domain) in a Jmjd1a co-IP assay. We subjected lysates
378 from mouse M12 B cells, which expresses endogenous OCA-B, to immunoprecipitation with Jmjd1a
379 antibodies, resulting in OCA-B co-IP (Fig. 6I, lane 3). Incubation of precipitated material with
380 scrambled or double point mutant peptides had no effect on OCA-B co-immunoprecipitation (lanes 4-
381 5), while the same concentration of JumOCA peptide efficiently blocked OCA-B recovery (lane 6).
382
383 **JumOCA protects NOD mice from newly-arisen T1D**
384 By the time symptoms arise in NOD mice, 90-95% of beta cells have been destroyed. Remaining beta
385 cells are rendered nonfunctional due to insulitis. Alleviating this inflammation provides a "honeymoon
386 period" during which glucose homeostasis can be restored. We treated 12-18 wk littermate female
387 NOD mice whose glucose levels were newly-risen above 225 mg/dL but still below 275 mg/dL with
388 three intravenous injections of 10 mg/kg JumOCA peptide or Tat-only peptide control. Injections were
389 spaced 12 hr apart. Immediately after the second injection and 4 hr after the final injection, blood

390 glucose was measured. Strikingly, JumOCA but not Tat-only or scrambled peptide reversed elevated
391 blood glucose (Fig. 7A). Islet T cell pro-inflammatory IFNγ and IL-17A cytokine production were
392 reduced by JumOCA peptide treatment compared to Tat-only controls (Fig. 7B,C). In contrast to the
393 pancreas, PLNs showed no change in T cell numbers or percentages (Fig. 7D) but similar decreases in
394 pro-inflammatory cytokine production (not shown).

395 Autoantigen-specific $CD8^+$ T cells in the PLNs of prediabetic, OCA-B deficient animals are
396 present but poorly activated by self-peptide (Fig. 3D,E). We treated animals with three injections of
397 JumOCA or scrambled peptide control, and stimulated PLN WBCs with IGRP self-peptides as in Fig.
398 3D. Significant reductions in IFN expression were observed in JumOCA-treated animals compared to
399 controls (Fig. 7E). Quantification from multiple mice is shown in Fig. 7F. These data show that
400 JumOCA peptide treatment decreases $CD8^+$ T cell autoreactivity within the PLNs, similar to genetic
401 OCA-B deletion. Cumulatively, these data provide evidence that targeting OCA-B is a valid strategy to
402 treat emerging T1D, and identify a first-generation inhibitor that is efficacious in vivo.

403 **Discussion**

404 Autoimmune therapies aim to inhibit autoreactivity while preserving normal immune function. Here
405 we show that genetic and pharmaceutical targeting of OCA-B blocks T1D in mouse models. Although
406 potentially autoreactive $CD8^+$ T cell specificities are still generated and appear in the PLNs of OCA-B
407 T cell deficient mice, they fail to become activated and do not accumulate in the pancreas. In contrast,
408 potentially autoreactive $CD4^+$ T cells are present but associated with anergic cell populations. OCA-B
409 is not expressed during thymic development or in naïve $CD4^+$ T cells, but is stably induced upon
410 activation. In contrast, OCA-B is expressed in naïve $CD8^+$ T cells and rapidy increased upon
411 activation.

412 In $CD4^+$ T cells, OCA-B associates with the POU-domain transcription factor Oct1 at ~150
413 immunomodulatory genes – among them *Il2*, *Ifng* and *Csf2* (*Gmcsf*). Unlike transcription factors such
414 as NF-AT, AP-1 and NF-kB that act as primary "on" switches, OCA-B removes inhibitory chromatin
415 modifications to establish permissive chromatin environments that allow for silent but previously
416 activated targets to be robustly expressed upon antigen re-encounter (Shakya et al., 2015; Shakya et al.,
417 2011). More specifically, OCA-B interacts with Jmjd1a, a histone lysine demethylase that removes
418 inhibitory histone H3 lysine 9 methyl marks. In vivo, OCA-B loss preserves T cell development and
419 pathogen response, but impairs the establishment of new central memory $CD4^+$ T cells. The few cells
420 that are formed respond poorly to antigen re-encounter (Shakya et al., 2015). Repeated antigen
421 encounters that drive high levels of proinflammatory cytokines are a key feature of autoimmunity. In
422 both mice and humans, memory or memory-like cells can underlie autoimmunity including T1D (Chee
423 et al., 2014; Kawakami et al., 2005; Yeo et al., 2018).

424 The NOD model of T1D is spontaneous but only partially penetrant, much like the human
425 disease (Parker et al., 2009). 60-80% of female NOD mice develop T1D in standard environments
426 (Makino et al., 1985). We find that prediabetic OCA-B T cell deficient NOD mice harbor normal T
427 cell numbers and TCR specificities in their PLNs, consistent with prior observations that OCA-B
428 deficient T cells are largely immunocompetent (Kim et al., 2019; Shakya et al., 2015). Nevertheless, T
429 cell conditional OCA-B knockouts are protected from spontaneous T1D. Whole-body NOD *Ocab*
430 knockouts are also protected from T1D. Prior work showed that OCA-B whole-body knockout protects
431 mice both from lupus-like disease mediated by loss of *Izkf3*/*Aiolos* (Sun et al., 2003), and in a
432 MOG/EAE model of multiple sclerosis (Ikegami et al., 2019). In contrast, a third study showed
433 exacerbation of systemic, antibody-driven autoimmunity in *Sanroque* mice (Chevrier et al., 2014). The
434 protective vs. exacerbating effects in whole body knockouts may be due to effects on class switching
435 and affinity maturation in germinal centers vs. effects on BCR repertoire (Casellas et al., 2002). A

436 whole body OCA-B knockout also reduces fat accumulation and insulin resistance in aged mice, likely
437 through ablation of B cell-mediated inflammation in white adipose tissue (Carter et al., 2018). T cell-
438 specific knockout of Oct1, a transcription factor with which OCA-B docks, blocks EAE but preserves
439 responses to infection with neurotropic viruses (Kim et al., 2019). Together these data show that in T
440 cells Oct1 and OCA-B promote autoimmunity including T1D, but that their role in B cells may be
441 more complex. OCA-B is typically expressed 50-100-fold higher in B cells compared to T cells. A
442 correctly calibrated dose of competitive inhibitor could therefore be used to selectively blunt T cell-
443 mediated autoimmunity.

444 scRNAseq experiments reveal decreased pancreatic neutrophil infiltration and an increased
445 percentages of T cells with naïve phenotypes in prediabetic OCA-B conditional knockouts. Gene
446 expression changes were identified consistent with antidiabetogenic effects of OCA-B T cell knockout.
447 For example, the remaining islet neutrophils in knockout mice show reductions in *Cxcl2* expression.
448 Cxcl2 is a potent neutrophil chemoattractant that promotes T1D in vivo (Citro et al., 2015; Diana and
449 Lehuen, 2014). Strikingly, OCA-B T cell deficient mice also lack T1D-associated TCR clones in their
450 activated/memory CD8 pool. Flow cytometry using class I tetramers show a significant reduction in
451 $CD8^+$ T cells specific for the $IGRP_{206-214}$ autoantigen. PLN $CD8^+$ T cells reactive to this and other
452 autoantigens show reduced reactivity to peptide stimulation ex vivo, suggesting that these autoreactive
453 $CD8^+$ cells are produced in the thymus but fail to become activated in the PLNs. In contrast, CD4
454 clonotypes associated with T1D are present in the pancreata, but associated with anergic gene
455 expression profiles. Consistently, OCA-B loss promotes $CD4^+$ T cell anergy in vitro. Loss of Oct1, the
456 transcription factor with which OCA-B docks, also augments anergic responses (Kim et al., 2019).

457 C57BL/6.RIP-mOVA and NOD.BDC2.5 transgenic mice are simplified monoclonal systems
458 that allow tracking of uniform T cell responses to antigens in vivo (Haskins, 2005). RIP-mOVA
459 expresses synthetic membranous chicken ovalbumin in thymic epithelial and pancreatic beta cells
460 (Kurts et al., 1996; Van Belle et al., 2009). Disease in can be induced in this model in 6-10 d by the
461 addition of OT-I T cells and infection with the OVA-expressing *Listeria*. OCA-B loss in host T cells
462 has no effect in this model. BDC2.5 autoreactive T cells migrate to the islets and cause insulitis
463 beginning at 3-4 weeks (Katz et al., 1993). Due in part to Tregs that have escaped allelic exclusion, in
464 many animals insulitis is limited and does not progress to T1D. However, transferring
465 $CD4^+CD62L^+V\beta^+$ or $CD4^+CD25^-$ T cells from BDC2.5 donor mice into NOD.SCID recipients also
466 results in rapid (7-10 d) disease onset (Berry and Waldner, 2013). Transplants from both control and
467 OCA-B null NOD/BDC2.5 mice results in disease with similar kinetics. Identical results were

468 generated by depleting $CD25^+$ Tregs, or by transplanting total $CD4^+$ T cells into immunodeficient
469 NCG recipient mice.
470 NOD.NY8.3 TCR transgenic mice carry a monoclonal CD8-restricted TCR directed towards
471 $IGRP_{206-214}$ and manifest spontaneous T1D (Verdaguer et al., 1997). Unlike transplantation models,
472 OCA-B T cell conditional NY8.3 mice show significant protection from spontaneous T1D.
473 Cumulatively, the results support a model in which OCA-B loss preserves T cell functionality while
474 desensitizing autoreactive T cells. This results in graded protection that drops off using models in
475 which protection is inseparable from immunodeficiency. These properties make OCA-B a promising
476 target for pharmaceutical inhibition.
477 Recent work indicates that the prevailing idea that transcription regulators and protein-protein
478 interactions are "undruggable" is erroneous (Antony-Debre et al., 2017; Green, 2016; Skwarczynska
479 and Ottmann, 2015; Zuber et al., 2011). Pre-clinical membrane-penetrating peptides have also been
480 developed that successfully target transcription factors such as BCL6 (Polo et al., 2004). We applied
481 rational-design principles to generate a membrane-permeable competitive peptide inhibitor of the
482 interaction between OCA-B and a downstream effector, Jmjd1a/Kdm3a. The sequence of the inhibitor,
483 termed JumOCA, does not coincide with other sequences in the human or mouse proteome and is not
484 predicted to be strongly immunogenic. JumOCA administration blunts newly-arisen T1D in NOD mice
485 and significantly reduces islet T cell cytokine production. Total T cell numbers were unaffected,
486 however PLN $CD8^+$ T cell autoreactivity to IGRP peptides was blunted, similar to T cell knockouts.
487 OCA-B levels in B cells are at least 50-fold higher than in T cells (Heng et al., 2008; Zwilling et al.,
488 1997), making it likely that the observed effects are due to inhibition in T cells. Consistently, three
489 JumOCA injections has no effect of splenic germinal center architecture (not shown), which is known
490 to depend OCA-B expression in B cells (Qin et al., 1998). More than three peptide injections results in
491 toxicity (not shown), complicating experiments testing T1D prevention and durable response. Tat-
492 conjugated peptides are known to be associated with toxicity (Caron et al., 2004; Krautwald et al.,
493 2004; Polo et al., 2004). While these peptides are unlikely to be used in a clinical setting, they offer
494 proof-of-principle for OCA-B as a therapeutic target, and can be used as tools for the further
495 development of therapeutics with the caveat that targeting this pathway would likely inhibit the
496 generation of new memory $CD4^+$ T cells.

Acknowledgements

We thank P. Santamaria, M. Williams, M. Bettini and F. Gounari for critical reading of the manuscript. We thank A. Chervonsky (U. Chicago) for the gift of NOD.CD4-cre mice. We thank J. Marvin and the University of Utah Health Sciences Center Flow Cytometry Core facility for assistance with flow cytometry, and D. Lum and the Preclinical Resource Core for immunodeficient mice. We thank M. Hanson and the University of Utah Health Sciences DNA/peptide synthesis core.

This work was supported by grants to DT from the Praespero Foundation, Juvenille Diabetes Research Foundation (1-INO-2018-647-A-N) and National Institutes of Health (R01-AI100873).

Author contributions: DT conceived the study and designed experiments, supervised the study, and provided administrative and material support. HK, AS, AI and JLJ acquired and interpreted the data. JP performed analysis of scRNAseq and TCR clonotype data. CG and NPL helped generate critical reagents. BDE, DH-CC, XH and PJ provided material and intellectual support. All authors were involved in writing, reviewing and revising the manuscript.

Disclosures: The authors declare that they have no conflicts of interest regarding this work.

512 **Materials and methods**

513 **Mice**

514 All animal experiments were approved by the University of Utah Institutional Animal Care and Use
515 Committee (IACUC approval 17-05008). NOD/ShiLtJ, NOD.Scid (NOD.Emv302/2.CB17-Prkdcscid),
516 BDC-2.5 TCR transgenic, NY8.3 TCR transgenic and all breeder mice were maintained in a specific
517 pathogen-free research colony. NCG (NOD-Prkdc^{em26Cd52}Il2rg^{em26Cd22}/NjuCrl) mice were purchased
518 from Charles River Laboratories. NOD.CD4-cre mice were a gift from Alexander Chervonsky
519 (University of Chicago). *Pou2af1*$^{tm1a(KOMP)Wtsi}$ mice were provided by the knockout mouse project
520 (KOMP) repository (University of California, Davis). Mice were derived from embryonic stem cell
521 clone EPD0761_3_B03, generated by the Wellcome Trust Sanger Institute. These cells were derived
522 from C57BL/6N mice, but subsequent mouse crosses were to C57BL/6J (>20 generations) for the RIP-
523 mOVA model and NOD (4 congenic backcrosses plus an additional backcross to NOD.CD4-cre). The
524 embryonic stem cells contain a CSD-targeted allele (Testa et al., 2004). The presence of WT (582 bp)
525 and Post-FLP (700 bp) alleles was determined by PCR using CSD-Pou2af1-F and CSD-Pou2af1-ttR
526 primers. The presence of the null (801 bp) allele was determined using CSD-Pou2af1-F and CSD-
527 Pou2af1-R primers. The presence of the floxed (359 bp) allele was determined using CSD-Lox-F and
528 CSD-Pou2af1-R primers. Primer sequences were as follows: CSD-Pou2af1-F,
529 5'TACAGAGAGACTAGACACGGTCTGC; CSD-Pou2af1-R,
530 5'GATGAGGACTCTGGGTTCAGAGAGG; CSD-loxF, 5'GAGATGGCGCAACGCAATTAATG;
531 CSD-Pou2af1-ttR, 5'AGAAGGCCTCGTTACACTCCTATGC.

532

533 **Backcrossing *Ocab* germline null and conditional mice to the NOD background**

534 To generate *Ocab*$^{-/-}$ and *Ocab* conditional mice on the NOD background, the previously described
535 C57BL/6 *Ocab* germline null allele (Kim et al., 1996) and the newly-generated *Ocab* conditional allele
536 were backcrossed to NOD ShiLt/J mice using congenic markers based on Mouse Genome Informatics
537 (http://www.informatics.jax.org) (Table S1).

538

539 **Diabetes development and assessment**

540 Diabetes was monitored using blood glucose test strips (Contour, Bayer). Mice with blood glucose
541 levels >250 mg/dL were considered diabetic.

542

543 **Leukocyte isolation and flow cytometry**

544 PLNs were disaggregated and passed through a nylon strainer. Pancreatic leukocytes were isolated as
545 described previously (Sitrin et al., 2013). Briefly, pancreata were chopped and digested using
546 collagenase IV (1 mg/mL, Gibco) in DMEM containing 1% fetal bovine serum (FBS, Rocky Mountain
547 Biologicals) and 10 units of DNase I for 15 min at 37°C. The digested tissues were passed through a 70
548 μm strainer. Red blood cells were lysed by ACK (Ammonium-Chloride-Potassium) lysis buffer (150
549 mM NH_4Cl, 10 mM $KHCO_3$, 0.1 mM Na_2EDTA). For intracellular cytokine staining, cell suspensions
550 in RPMI medium supplemented with 10% FBS were re-stimulated for 4 hr with phorbol 12-myristate
551 13-acetate (PMA, Sigma, 50 ng/mL) and ionomycin (Sigma, 1 μg/mL) in the presence of brefeldin A
552 (GolgiPlug, BD Bioscience, 1 μl/ml), and fixed by cell fixation/permeabilization solution (BD
553 Cytofix/Cytoperm) according to the manufacturer's protocol. Antibodies used for flow cytometry were
554 as follows: FITC-conjugated anti-mouse CD4, PE-conjugated anti-mouse CD45, PE-conjugated anti-
555 mouse FR4 (BioLegend), PerCP-conjugated anti-mouse CD8a, APC-conjugated anti-mouse IFNγ, PE-
556 conjugated anti-mouse IL-17, PerCP-conjugated anti-mouse CD11b, APC-conjugated anti-mouse
557 F4/80, PE-conjugated anti-mouse Gr-1, PE-conjugated anti-mouse ICOS (eBioscience), PerCP-
558 conjugated anti-mouse FoxP3, V450-conjugated anti-mouse CD73 (BD Bioscience) and FITC-
559 conjugated anti-mouse Vβ8.1/8.2 (Invitrogen). A FACS Canto II (BD Biosciences) was utilized for
560 flow cytometry, and FlowJo software was used for analyses.
561
562 **T cell adoptive transfer**
563 6–8 wk old NOD.Scid recipient mice were injected retro-orbitally with 2×10^5 of splenic $CD4^+CD25^-$ T
564 cells from prediabetic *Ocab*$^{-/-}$ or *Ocab*$^{+/+}$ NOD.BDC2.5 donors (6–8 wk old, sex-matched). T cells
565 were purified using a $CD4^+CD25^+$ T cell isolation kit (Miltenyi). For $CD4^+CD25^+$ T cells, 1.5×10^6
566 purified splenic $CD4^+$ T cells from prediabetic, BDC2.5 transgenic NOD.*Ocab*$^{-/-}$ or NOD.*Ocab*$^{+/+}$
567 mice were transferred to sex-matched 6-8 wk old NCG recipients (University of Utah Preclinical
568 Resource Core) as previously described (Presa et al., 2015). For total splenic transfer experiments,
569 5×10^6 splenocytes from prediabetic NOD.*Ocab*$^{fl/fl}$ or NOD.*Ocab*$^{fl/fl}$CD4-cre mice were transferred into
570 sex-matched 6-8 wk NOD.Scid recipients mice as described previously (Presa et al., 2015).
571
572 **In vitro T cell culture**
573 For anergic cell induction, spleens were harvested from NOD.*Ocab*$^{fl/fl}$CD4-cre or control NOD.*Ocab*$^{fl/fl}$
574 animals. Single-cell suspensions were generated by grinding and passage through 70 μm strainers.
575 Cells were isolated using a mouse $CD4^+$ T cell isolation kit (Miltenyi Biotec), and stimulated with

576 5 μg/ml plate-bound anti-CD3ε (BD Bioscience) ± 2 μg/ml anti-CD28 antibody (eBioscience) as
577 described previously (Kim et al., 2019). For OCA-B inhibitor peptide treatments, cells were isolated
578 from WT C57BL/6 spleens using a mouse naïve $CD4^+$ T cell isolation kit (Miltenyi Biotec) and
579 cultured as described previously (Shakya et al., 2011). Indicated concentrations of peptides were
580 incubated with cells, with media changes every 2 days after primary stimulation. Activation of
581 C57BL/6 $CD4^+$ cells and subsequent profiling of anergic responses was performed identically to (Kim
582 et al., 2019). For peptide restimulation, total WBCs from PNLs were incubated with 10 μg/mL
583 specific peptide for 4 hr in the presence of brefeldin A. The peptides used were as follows: $GAD65_{206-}$
584 $_{214}$, TYEIAPVFV; $GAD65_{546-554}$, SYQPLGDKV; $IGRP_{21-29}$, TYYGFLNFM; $IGRP_{206-214}$,
585 VYLKTNVFL; $IGRP_{225-233}$, LRLFGIDLL; $IGRP_{241-249}$, KWCANPDWI; $IGRP_{324-332}$, SFCKSASIP.
586 Cells were then fixed and stained for flow cytometry.
587
588 **Single-cell RNA sequencing**
589 $CD3^+$ T cells were isolated from 8 wk NOD.*Ocab*$^{fl/fl}$ or NOD.*Ocab*$^{fl/fl}$CD4-cre females using a pan T
590 cell isolation kit (Miltenyi). $CD45^+$ pancreatic leukocytes were isolated from 12 wk NOD.*Ocab*$^{fl/fl}$ or
591 NOD.*Ocab*$^{fl/fl}$CD4-cre females were isolated by flow cytometry using a FACS Aria (Becton-
592 Dickinson). For each condition, cells were isolated from three mice and combined. Cells were
593 processed using the 10X Genomics Chromium platform according the manufacturer's instructions.
594 Paired-end high-throughput sequencing (125 cycles) was performed via an Illumina NovaSeq
595 instrument. Sequencing reads were processed by using 10X Genomics CellRanger pipeline and further
596 analyzed using the Seurat R package. Analysis of cells used a standard filtering protocol removing
597 cells with unique feature counts of >4,000 or <500, as well as cells with >5% mitochondrial counts
598 (indicative of dead cells). No more than 15% of total cells were removed by this process. Cells were
599 subjected to unsupervised hierarchical clustering followed by uniform manifold approximation and
600 projection (UMAP) to visualize clusters with similar gene expression and their relative positions.
601
602 **Tetramer staining**
603 H-$2K^d$ mouse $IGRP_{206-214}$ tetramers (Mouse NRP-V7 mimotope KYNKANVFL) conjugated to APC
604 or PE were synthesized by the NIH tetramer core facility and were a gift of Dr. Maria Bettini
605 (University of Utah).
606
607 **OCA-B mutagenesis and Co-IP**

608 For generation of the OCA-B double point mutant, a plasmid transiently expressing human OCA-B,
609 pCATCH-Bob.1 (Gstaiger et al., 1995), was sequentially mutagenized using QuickChange
610 (ThermoFisher). Correct mutagenesis was confirmed by resequencing. HCT116 lysate preparation, co-
611 immunoprecipitation of OCA-B and endogenous Jmjd1a, and immunoblot detection was performed
612 using the same conditions as described (Shakya et al., 2015). For co-IP using M12 cells, lysis buffer
613 consisted of 50 mM Tris-Cl, pH 7.4, 150mM NaCl, 0.5%NP-40, 1 mM EDTA, 1 mM EGTA, plus
614 protease/phosphatase inhibitors (PhosSTOP, Roche). Lysates were incubated with 2.5 µg Jmjd1A
615 antibody (Bethyl) and protein-G Dynabeads (ThermoFisher) in lysis buffer containing 20% glycerol
616 overnight at 4°C. After overnight incubation, the indicated concentrations of peptide or PBS vehicle
617 was added and incubated for a further 3 hr at 4°C prior to bead precipitation and washing 3× in lysis
618 buffer plus 20% glycerol. Co-precipitated OCA-B was analyzed by SDS-PAGE and immunoblot.
619

620 **OCA-B inhibitor peptide synthesis**

621 Unique chemically synthesized peptide sequences were as follows: Peptide#1, ARPYQGVRVKEPVK;
622 Peptide#2/JumOCA, VKELLRRKRGH; Peptide#3, ARPYQGVRVKEPVKELLRRKRGH; Scrambled
623 peptide, VLREKGKRHLR. Peptides were synthesized with and without a covalent C-terminal linker
624 and Tat membrane-penetrating peptide (GSG-GRKKRRQRRRGY). Fmoc protected amino acids were
625 obtained from Protein Technologies Inc. 1-[Bis(dimethylamino)methylene]-1H-1,2,3-triazolo[4,5-
626 b]pyridinium 3-oxid hexafluorophosphate (HATU) was purchased from Chemimpex Inc. H-Rink-
627 Amide-ChemMatrix (RAM) was purchased from Biotage. N,N-diisopropylethylamine (DIEA),
628 dichloromethane (DCM), triisopropylsilane (TIS) were purchased from Sigma Aldrich.
629 Dimethylformamide (DMF), trifluoroacetic acid (TFA), acetonitrile (ACN), and ethyl ether were
630 purchased from Fisher Scientific. Peptides were synthesized using automated Fmoc SPPS chemistry
631 (Syro I). Briefly, 220 mg of RAM resin (Loading = 0.45 mmol/g) was swelled in DCM for 15 min and
632 followed by adding a solution of specific Fmoc protected amino acid (AA = 0.1 mmol, DIEA = 0.2
633 mmol in DCM = 4 mL) and incubated at room temperature for 1.5 h. The resin was washed with DMF
634 and DCM and incubated with 5 mL of DCM containing 16% v/v MeOH and 8% v/v DIEA for 5 min.
635 This action was repeated 5 times before thoroughly washing with DCM and DMF. Coupling reactions
636 were performed using HATU (5 eq.), DIPEA (10 eq.) and amino acid (5 eq.) in DMF with 15 min
637 heating to 70°C (50°C for Cys). Deprotection was performed using 20% (v/v) piperidine in DMF, 5
638 min at room temperature for 2 rounds. Peptides were cleaved from the resin by treatment with a
639 cocktail buffer (3 mL/0.1 mmol, TFA:H2O:TIS:EDT = 95:2:2:1) for 2.5 h. Peptide-TFA solution was

640 then filtered and precipitated in cold ether, centrifuged, washed with ether twice and vacuum-dried.
641 The crude product was then purified by RP HPLC. Peptide characterization was performed by LC/MS
642 on an Xbridge C18 5 µm (50 x 2.1 mm) column at 0.4 mL/min with a water/acetonitrile gradient in
643 0.1% formic acid on an Agilent 6120 Quadrupole LC/MS system. Fractions collected from HPLC runs
644 were also analyzed by LC/MS. The purified fractions containing the targeted product were collected
645 and lyophilized using a Labconco Freeze Dryer. All samples were analyzed by the following
646 conditions: Preparative reverse phase HPLC of crude peptides was performed on a Jupiter 5 µ C18 300
647 Å (250×10 mm) column at 3 mL/min with a water/acetonitrile (ACN) gradient in 0.1% TFA on an
648 Agilent 1260 HPLC system. Purity, isomer co-injection and stability checks were performed on HPLC
649 on Phenomenex Gemini C18 3 µm (110 Å 150×3 mm) column.
650
651 **OCA-B inhibitor peptide treatment**
652 Anesthetized prediabetic WT NOD females with glucose levels newly-risen to between 225 to 275
653 mg/dL were treated with 10 mg/kg inhibitor or control peptides by intravenous (retro-orbital) injection,
654 3 times every 12 hr. Blood glucose levels were measured after the 2nd and 3rd injection. 4 hr after the
655 last injection, pancreata and PLNs were collected and cell populations were analyzed by flow
656 cytometry.
657
658 **Histology**
659 Formalin-fixed pancreatic tissues were embedded in paraffin. H&E-stained sections were scored for
660 islet inflammation based on published precedents (Zhang et al., 2007): 0, sparse surrounding sentinel
661 leukocytes, no insulitis; 1, peri-islet leukocytes; 2, some islet leukocytes, <50% of islet area; 3, islet
662 insulitis with >50% of islet area occupied by leukocytes; 4, islets destroyed with fibrotic remnants.
663
664 **Statistical analyses**
665 All error bars denote ±SEM. Two-tailed student T-tests were used to ascribe statistical significance.
666 For all figures, *=$p \leq 0.05$; **=$p \leq 0.005$; ***=$p \leq 0.001$; ****=$p \leq 0.0001$.

667 **Figure legends**

668 Figure 1. **Loss of OCA-B protects NOD mice from T1D. (A)** Kaplan-Meier plot of diabetes-free
669 survival in littermate female NOD.*Ocab*$^{fl/fl}$CD4-cre (n=12) and NOD.*Ocab*$^{fl/fl}$ (n=14) mice. HR=hazard
670 ratio. **(B)** Average blood glucose levels from mice shown in panel A. **(C)** Percent diabetes-free
671 survival in germline knockout NOD.*Ocab*$^{-/-}$ (n=16) and control NOD.*Ocab*$^{+/+}$ (n=17) mice was
672 plotted. **(D)** Pancreatic islet leukocytes were isolated from 8 wk- or 24 wk-old littermate female
673 NOD.*Ocab*$^{fl/fl}$CD4-cre (8 wk; n=3, 24 wk; n=5) or NOD.*Ocab*$^{fl/fl}$ (8 wk; n=3, 24 wk; n=4) mice and
674 analyzed by flow cytometry. Mean CD45$^+$CD11b$^+$F4/80$^+$ cell frequencies are depicted. **(E)**
675 Frequencies of CD45$^+$CD11b$^+$F4/80$^+$ cells from representative animals in D are shown. Plots were
676 gated on CD45. **(F)** Mean percentages of total pancreatic-infiltrating CD8$^+$ T cell in 9 experimental
677 NOD.*Ocab*$^{fl/fl}$CD4-cre or 11 littermate control NOD.*Ocab*$^{fl/fl}$ 12 wk-old mice are plotted. Cells were
678 gated on CD45. **(G)** IFNγ expressing CD8$^+$ T cell percentages in 16 wk old-NOD.*Ocab*$^{fl/fl}$CD4-cre
679 (n=3) and littermate control islets (n=5) are shown.

680

681 Figure 2. **T cell conditional OCA-B loss reduces the numbers of activated, autoreactive**
682 **pancreatic islet T cells. (A)** scRNAseq using total islet CD45$^+$ cells from prediabetic
683 NOD.*Ocab*$^{fl/fl}$CD4-cre or littermate control NOD.*Ocab*$^{fl/fl}$ mice (n=4 for each group). Cell populations
684 were plotted using UMAP (Seurat R package) and percentages in each cluster are shown for each
685 genotype. Clusters were identified using the Seurat R package function FindMarkers. **(B)** 4 clusters
686 from A were analyzed for differential gene expression. Identified genes are shown as a scatter plot.
687 Significantly differentially expressed genes (adjusted *p*-value <0.05) are shown in red. For *Cxcl2* in
688 neutrophils, $p=3.75\times10^{-6}$, adjusted $p=0.055$. **(C)** UMAP plots similar to A, except cells expressing
689 TCR clonotype 13-3 are shown. The non-naïve (activated+memory) CD8$^+$ cell population identified in
690 A is shown in red. **(D)** Percent contribution of the top 6 identified TCR clonotypes to total
691 activated+memory CD8$^+$ cells is shown. V genes comprising the clonotypes are shown below. **(E)**
692 Cells positive for clonotypes 1-5 are shown for two clusters, non-naïve (activated+memory) CD8$^+$ T
693 cells and CTLA4$^+$FR4$^+$ anergic cells (consisting of mostly CD4$^+$ cells). For each cluster, positive cells
694 are shown in dark blue. An overlay of control and OCA-B deficient cell populations is shown. Each
695 clonotype is only observed in a single genotype (panel D), allowing all cells to be mapped back
696 entirely to OCA-B deficient (clonotypes 1 and 4) or control (clonotypes 2, 3 and 5).

697

698 Figure 3. **Autoantigen-specific CD8+ cells become nonreactive and fail to infiltrate islets in the**
699 **OCA-B deficient condition. (A)** Pancreatic leukocytes were isolated from prediabetic 12 wk
700 littermate female NOD.*Ocab*$^{fl/fl}$CD4-cre (n=9) or NOD.*Ocab*$^{fl/fl}$ (n=10) mice and analyzed by flow
701 cytometry. Representative plots (left) and total CD8$^+$Vβ8.1$^+$ T cell numbers (right) are shown. **(B)**
702 PLN leukocytes were isolated from same mice (NOD.*Ocab*$^{fl/fl}$CD4-cre, n=7 or NOD.*Ocab*$^{fl/fl}$, n=5) in
703 A. Representative plots (left) and total CD8$^+$Vβ8.1$^+$ T cell frequencies (right) are shown. **(C)**
704 Representative plots (left) and total cell numbers (right) of CD8$^+$Vβ8.1$^+$ H-2K^d IGRP$_{206-214}$ tetramer-
705 positive islet T cells are depicted from NOD.*Ocab*$^{fl/fl}$CD4-cre (n=9) or NOD.*Ocab*$^{fl/fl}$ (n=10). **(D)** Total
706 PLN WBCs were isolated from prediabetic 12 wk-old littermate NOD.*Ocab*$^{-/-}$ or NOD.*Ocab*$^{+/+}$ mice
707 and re-stimulated with IGRP peptides (IGRP$_{206-214}$ or IGRP$_{225-233}$). Cells were analyzed for IFNγ
708 expression by flow cytometry. **(E)** Mean percentages of cells expressing IFNγ from 9 experiments (3
709 replicates from 3 *Ocab*$^{+/+}$ and 3 *Ocab*$^{-/-}$ mice) for the peptides in D, as well as two GAD65 peptides
710 (206-214 and 546-554) and three additional IGRP peptides (21-29, 241-249 and 324-332).
711
712 Figure 4. **OCA-B loss protects NOD mice from T1D in spontaneous and polyclonal splenocyte**
713 **transfer models but not monoclonal transfer models. (A)** 2×10^5 purified CD4$^+$CD25$^-$ splenic T cells
714 from NOD.BDC2.5.*Ocab*$^{-/-}$ or control NOD.BDC2.5.*Ocab*$^{+/+}$ donors were injected retro-orbitally into
715 NOD.Scid (n=6 for each group) mice. Diabetes-free survival is shown. **(B)** 1.5×10^6 purified splenic
716 total CD4$^+$ T cells from NOD.BDC2.5.*Ocab*$^{-/-}$ or control donors were transferred into NCG mice (n=5
717 for each group). Mice were monitored for diabetes development. **(C)** Total NOD splenocytes (5×10^6)
718 from prediabetic 6- to 8-wk-old NOD.*Ocab*$^{fl/fl}$CD4-cre or control NOD.*Ocab*$^{fl/fl}$ donors were
719 adoptively transferred into sex-matched NOD.Scid (n=7 for each group) recipients. T1D-free survival
720 is shown. **(D)** 13 wk post-transfer, the proportion of IFNγ-expressing islet CD8$^+$ T cells was assessed
721 by flow cytometry from mice in C. **(E)** Pancreata from the same mice as in D were fixed, sectioned
722 and H&E stained. Pathological scores are shown based on 6-7 islets/slide, 3 slides/mouse and 3
723 mice/group (>60 islets/group). **(F)** Example pancreatic images from endpoint animals. Yellow arrows
724 indicate islet positions. Images were collected at 10× magnification. **(G)** The *Ocab* null allele was
725 crossed to NY8.3 TCR transgenic mice. Spontaneous T1D was measured in female *Ocab*$^{-/-}$ (n=20) or
726 control *Ocab*$^{+/+}$ (n=12) littermates. **(H)** Naïve CD4$^+$ or CD8$^+$ T cells (CD8a^{neg} or
727 CD4^{neg},CD11b^{neg},CD45R^{neg},DX5^{neg},Ter-119^{neg},CD44^{lo}) were isolated from C57BL/6 spleens and
728 stimulated for up to 2 d in vitro using anti-CD3ε and CD28 antibodies. Cells were then washed and
729 replated in the presence of exogenous IL-2. After 8 d rest in culture, cells were restimulated for 6 hr.

730 Lysates were prepared from each step and subjected to OCA-B immunoblotting to assess changes in
731 expression. Oct1 and β-actin are shown as controls.
732
733 Figure 5. **OCA-B loss in CD4$^+$ T cells increases anergy in vitro. (A)** Naïve CD4$^+$ C57BL/6 T cells
734 were stimulated in vitro for 24 hr with anti-CD3ε antibodies ± co-stimulation with CD28 antibodies.
735 Lysates were prepared and subjected to immunoblotting using OCA-B antibodies. β-actin is shown as
736 a loading control. **(B)** Naïve OCA-B deficient and control CD4$^+$ T cells were stimulated in vitro with
737 anti-CD3ε antibodies. 48 hr later, the cells were re-stimulated with PMA and ionomycin for 6 hr in the
738 presence of brefeldin A, stained for intracellular IL-2 and analyzed by flow cytometry. Cells were
739 gated on CD4 and CD44. **(C)** Quantitation using independently purified cells from the spleens of 4
740 mice treated similar to B. **(D)** Naïve OCA-B deficient and littermate control splenic CD4$^+$ T cells from
741 6 wk-old NOD mice were stimulated for 2 d in vitro with indicated antibodies, replated and rested in
742 the absence of antibody for 2 d, and analyzed by flow cytometry. Mean FR4^{hi} CD73^{hi}CD4$^+$CD44$^+$ cell
743 frequencies are shown using independently purified cells from the spleens of 2 mice, with 4
744 independent culture replicates performed for each mouse (n=8). **(E)** Similar to D, except frequencies of
745 CD4$^+$CD44$^+$ICOS$^+$ cells are plotted. **(F)** Similar to D, except average percentage of
746 CD4$^+$CD44$^+$CD25$^+$ cells are plotted.
747
748 Figure 6. **Design and validation of OCA-B peptide inhibitors. (A)** OCA-B N-terminus (residues 16
749 and 38)/Oct1 DNA binding domain/octamer binding DNA co-crystal structure (PDB ID 1CQT)
750 (Green, 2016). Gray: DNA. Green: Oct1 DNA binding domain. Cyan: OCA-B. Red dashed line shows
751 position of the Oct1 linker domain. **(B)** Top alignment of the human androgen receptor (AR) isoform
752 transcript variant 1 (Sequence ID: ADD26780.1) co-activator interaction domain (residues 698-721)
753 with full-length human Oct1 and OCA-B. The aligned regions are from the Oct1 linker domain and
754 OCA-B N-terminus. Green serines: putative ERK phospho-acceptor sites. Yellow: similar or identical
755 amino acids. Asterisks: known human point mutations that block coactivator binding and cause
756 androgen insensitivity syndrome in humans. Pairwise alignments were performed using the FASTA
757 algorithm (https://embnet.vital-it.ch/software/LALIGN_form.html) and trimmed for 3-way overlap.
758 **(C)** Alignment of human and mouse primary OCA-B peptide sequences. **(D)** Co-IP of Jmjd1a with
759 L31A/R34A double point-mutant OCA-B and wild-type control. HCT116 cells transfected with WT or
760 mutant OCA-B constructs were used. Protein expression was checked 48 hrs after transfection by
761 Western blotting. 50 μg input protein was loaded in lanes 1-3. **(E)** Indicated peptide sequences were

762 synthesized as C-terminal Tat fusions for membrane permeability. Arrows indicate position of mutant
763 in B and D. **(F)** *Il2* mRNA expression in primary naïve $CD4^+$ T cells treated with 50 μM JumOCA
764 peptide was measured relative to β-actin internal standard by RT-qPCR. Cells were stimulated with
765 CD3ε/CD28 antibodies for 2 d, rested for a further 8 d in the presence of exogenous recombinant IL-2,
766 and restimulated for 6 hr. Peptide was included during resting and restimulation only, and replaced
767 every other day with media changes. **(G)** IL-2 cytokine expression in primary naïve $CD4^+$ T cells
768 cultured with 50μM peptide at initial treatment, and with 25μM peptide from the secondary treatment
769 was measured by flow cytometry. Cells were treated similarly to F except collection, brefeldin A
770 treatment and processing for flow cytometry occurred 24 hr post-restimulation. **(H)** $CD4^+CD44^+IL2^+$ T
771 cell frequencies from representative samples in G. Plots were gated on CD4 and CD44. **(I)** Peptide
772 effects on the interaction between OCA-B and Jmjd1a was measured by co-immunoprecipitation. M12
773 B cells were used. After incubation with protein-G beads, 0.2 μg/μL control scrambled (Scram),
774 double point mutant (DM) peptide or JumOCA peptide were added for a further 3 hr prior to
775 precipitation and washing. 1% input (lane 1) is shown as a control.
776
777 Figure 7. **OCA-B inhibitor peptide injections protect NOD mice from newly-arisen diabetes. (A)** 3
778 doses of 10 mg/kg JumOCA (n=4), Tat only (n=6) or scrambled peptide (n=3) were injected retro-
779 orbitally every 12 hr into 12-18 wk-old NOD female littermate mice whose glucose levels were newly-
780 risen above 225 mg/dL but still below 275 mg/dL. Glucose levels are shown immediately before the
781 first injection, after the second injection and 4 hr after the final injection. **(B)** 12 hr after the last
782 injection of peptides in A, PLN $CD4^+$ and $CD8^+$ T cell percentages were analyzed by flow cytometry.
783 Mean of islet IL-17 expressing T cells were analyzed by flow cytometry and plotted. **(C)** Similar
784 analysis as B except for IFNγ. **(D)** Percentages of PLN $CD4^+$ and $CD8^+$ T cells. **(E)** NOD mice were
785 treated with 3 intravenous peptide injections as before, except that 12-wk pre-diabetic mice were used
786 and scrambled peptide was additionally included as a control. 4 hr after the final injection, PLN WBCs
787 were stimulated with IGRP peptides and brefeldin A for 4 hr, stained for IFNγ and analyzed by flow
788 cytometry as in Figure 3D. Representative animals are shown. **(F)** Mean percentages of cells
789 expressing IFNγ from 6 experiments.

790 **Supplemental information**
791
792 **Document S1.** Figs. S1-S5
793
794 **Table S1.** Loci for type 1 diabetes susceptibility and resistance in NOD/ShiLtJ mice, and
795 oligonucleotide primer-pairs used for PCR amplification of *Idd* loci microsatellite markers, related to
796 Supplemental Figure S1
797
798 **Table S2.** Gene expression comparisons in T cells taken from PLNs of 8 week-old NOD.*Ocab*$^{fl/fl}$CD4-
799 cre and NOD.*Ocab*$^{fl/fl}$ littermate controls, related to Supplemental Figure S2
800
801 **Table S3.** Expression levels of *Ccl1* mRNA in naïve, stimulated, rested and re-stimulated OCA-
802 B/Pou2af1-deficient T cells relative to controls, related to Figure 1
803
804 **Table S4.** Gene expression comparisons in total CD45^{+} cells taken from pancreatic islets of 12 week-
805 old prediabetic NOD.*Ocab*$^{fl/fl}$CD4-cre and NOD.*Ocab*$^{fl/fl}$ littermate controls, related to Figure 2

806 **References**

807 Antony-Debre, I., A. Paul, J. Leite, K. Mitchell, H.M. Kim, L.A. Carvajal, T.I. Todorova, K. Huang, A. Kumar, A.A.
808 Farahat, B. Bartholdy, S.R. Narayanagari, J. Chen, A. Ambesi-Impiombato, A.A. Ferrando, I. Mantzaris,
809 E. Gavathiotis, A. Verma, B. Will, D.W. Boykin, W.D. Wilson, G.M. Poon, and U. Steidl. 2017.
810 Pharmacological inhibition of the transcription factor PU.1 in leukemia. *J Clin Invest* 127:4297-4313.
811 Berry, G., and H. Waldner. 2013. Accelerated type 1 diabetes induction in mice by adoptive transfer of
812 diabetogenic CD4+ T cells. *J Vis Exp* e50389.
813 Cantor, J., and K. Haskins. 2007. Recruitment and activation of macrophages by pathogenic CD4 T cells in type
814 1 diabetes: evidence for involvement of CCR8 and CCL1. *J Immunol* 179:5760-5767.
815 Caron, N.J., S.P. Quenneville, and J.P. Tremblay. 2004. Endosome disruption enhances the functional nuclear
816 delivery of Tat-fusion proteins. *Biochem Biophys Res Commun* 319:12-20.
817 Carter, S., S. Miard, A. Caron, S. Sallé-Lefort, P. St-Pierre, F.F. Anhê, E. Lavoie-Charland, P. Blais-Lecours, M.C.
818 Drolet, J.S. Lefebvre, J. Lacombe, Y. Deshaies, J. Couet, M. Laplante, M. Ferron, Y. Bossé, A. Marette, D.
819 Richard, D. Marsolais, and F. Picard. 2018. Loss of OcaB Prevents Age-Induced Fat Accretion and Insulin
820 Resistance by Altering B-Lymphocyte Transition and Promoting Energy Expenditure. *Diabetes* 67:1285-
821 1296.
822 Casellas, R., M. Jankovic, G. Meyer, A. Gazumyan, Y. Luo, R. Roeder, and M. Nussenzweig. 2002. OcaB is
823 required for normal transcription and V(D)J recombination of a subset of immunoglobulin kappa
824 genes. *Cell* 110:575-585.
825 Chai, J.G., and R.I. Lechler. 1997. Immobilized anti-CD3 mAb induces anergy in murine naive and memory CD4+
826 T cells in vitro. *Int Immunol* 9:935-944.
827 Chasman, D., K. Cepek, P.A. Sharp, and C.O. Pabo. 1999. Crystal structure of an OCA-B peptide bound to an
828 Oct-1 POU domain/octamer DNA complex: specific recognition of a protein-DNA interface. *Genes Dev*
829 13:2650-2657.
830 Chee, J., H.J. Ko, A. Skowera, G. Jhala, T. Catterall, K.L. Graham, R.M. Sutherland, H.E. Thomas, A.M. Lew, M.
831 Peakman, T.W. Kay, and B. Krishnamurthy. 2014. Effector-memory T cells develop in islets and report
832 islet pathology in type 1 diabetes. *J Immunol* 192:572-580.
833 Chevrier, S., T. Kratina, D. Emslie, A. Karnowski, and L.M. Corcoran. 2014. Germinal center-independent, IgM-
834 mediated autoimmunity in sanroque mice lacking Obf1. *Immunol Cell Biol* 92:12-19.
835 Citro, A., A. Valle, E. Cantarelli, A. Mercalli, S. Pellegrini, D. Liberati, L. Daffonchio, O. Kastsiuchenka, P.A.
836 Ruffini, M. Battaglia, M. Allegretti, and L. Piemonti. 2015. CXCR1/2 inhibition blocks and reverses type
837 1 diabetes in mice. *Diabetes* 64:1329-1340.
838 Cooke, D.W., and L. Plotnick. 2008. Type 1 diabetes mellitus in pediatrics. *Pediatr Rev* 29:374-384; quiz 385.
839 Cunninghame Graham, D.S., A.K. Wong, N.J. McHugh, J.C. Whittaker, and T.J. Vyse. 2006. Evidence for unique
840 association signals in SLE at the CD28-CTLA4-ICOS locus in a family-based study. *Hum Mol Genet*
841 15:3195-3205.
842 Delong, T., T.A. Wiles, R.L. Baker, B. Bradley, G. Barbour, R. Reisdorph, M. Armstrong, R.L. Powell, N. Reisdorph,
843 N. Kumar, C.M. Elso, M. DeNicola, R. Bottino, A.C. Powers, D.M. Harlan, S.C. Kent, S.I. Mannering, and
844 K. Haskins. 2016. Pathogenic CD4 T cells in type 1 diabetes recognize epitopes formed by peptide
845 fusion. *Science* 351:711-714.
846 Diana, J., and A. Lehuen. 2014. Macrophages and beta-cells are responsible for CXCR2-mediated neutrophil
847 infiltration of the pancreas during autoimmune diabetes. *EMBO Mol Med* 6:1090-1104.
848 Dong, C., A.E. Juedes, U.A. Temann, S. Shresta, J.P. Allison, N.H. Ruddle, and R.A. Flavell. 2001. ICOS co-
849 stimulatory receptor is essential for T-cell activation and function. *Nature* 409:97-101.
850 Dong, C., and R.I. Nurieva. 2003. Regulation of immune and autoimmune responses by ICOS. *J Autoimmun*
851 21:255-260.
852 Farh, K.K., A. Marson, J. Zhu, M. Kleinewietfeld, W.J. Housley, S. Beik, N. Shoresh, H. Whitton, R.J. Ryan, A.A.
853 Shishkin, M. Hatan, M.J. Carrasco-Alfonso, D. Mayer, C.J. Luckey, N.A. Patsopoulos, P.L. De Jager, V.K.

854 Kuchroo, C.B. Epstein, M.J. Daly, D.A. Hafler, and B.E. Bernstein. 2015. Genetic and epigenetic fine
855 mapping of causal autoimmune disease variants. *Nature* 518:337-343.
856 Games Collaborative, G., M. Ban, D. Booth, R. Heard, G. Stewart, A. Goris, K. Vandenbroeck, B. Dubois, M.
857 Laaksonen, J. Ilonen, M. Alizadeh, G. Edan, M.C. Babron, D. Brassat, M. Clanet, I. Cournu-Rebeix, B.
858 Fontaine, G. Semana, R. Goedde, J. Epplen, A. Weber, C. Infante-Duarte, F. Zipp, C. Rajda, K. Bencsik, L.
859 Vecsei, S. Heggarty, C. Graham, S. Hawkins, M. Liguori, P. Momigliano-Richiardi, D. Caputo, L.M.
860 Grimaldi, M. Leone, L. Massacesi, C. Milanese, M. Salvetti, G. Savettieri, M. Trojano, B. Bielecki, M.P.
861 Mycko, K. Selmaj, M. Santos, P. Maciel, C. Pereira, A. Silva, B.M. Silva, F. Coraddu, M.G. Marrosu, E.
862 Akesson, J. Hillert, P. Datta, A. Oturai, H.F. Harbo, A. Spurkland, R. Goertsches, P. Villoslada, M.
863 Eraksoy, A. Hensiek, A. Compston, E. Setakis, J. Gray, T.W. Yeo, and S. Sawcer. 2006. Linkage
864 disequilibrium screening for multiple sclerosis implicates JAG1 and POU2AF1 as susceptibility genes in
865 Europeans. *J Neuroimmunol* 179:108-116.
866 Green, D.R. 2016. A BH3 Mimetic for Killing Cancer Cells. *Cell* 165:1560.
867 Gstaiger, M., O. Georgiev, H. van Leeuwen, P. van der Vliet, and W. Schaffner. 1996. The B cell coactivator
868 Bob1 shows DNA sequence-dependent complex formation with Oct-1/Oct-2 factors, leading to
869 differential promoter activation. *EMBO J* 15:2781-2790.
870 Gstaiger, M., L. Knoepfel, O. Georgiev, W. Schaffner, and C.M. Hovens. 1995. A B-cell coactivator of octamer-
871 binding transcription factors. *Nature* 373:360-362.
872 Haskins, K. 2005. Pathogenic T-cell clones in autoimmune diabetes: more lessons from the NOD mouse. *Adv*
873 *Immunol* 87:123-162.
874 Hattori, M., J.B. Buse, R.A. Jackson, L. Glimcher, M.E. Dorf, M. Minami, S. Makino, K. Moriwaki, H. Kuzuya, H.
875 Imura, and et al. 1986. The NOD mouse: recessive diabetogenic gene in the major histocompatibility
876 complex. *Science* 231:733-735.
877 Heng, T.S., M.W. Painter, and C. Immunological Genome Project. 2008. The Immunological Genome Project:
878 networks of gene expression in immune cells. *Nat Immunol* 9:1091-1094.
879 Ikegami, I., H. Takaki, S. Kamiya, R. Kamekura, and S. Ichimiya. 2019. Bob1 enhances RORgammat-mediated IL-
880 17A expression in Th17cells through interaction with RORgammat. *Biochem Biophys Res Commun*
881 514:1167-1171.
882 Kalekar, L.A., S.E. Schmiel, S.L. Nandiwada, W.Y. Lam, L.O. Barsness, N. Zhang, G.L. Stritesky, D. Malhotra, K.E.
883 Pauken, J.L. Linehan, M.G. O'Sullivan, B.T. Fife, K.A. Hogquist, M.K. Jenkins, and D.L. Mueller. 2016.
884 CD4(+) T cell anergy prevents autoimmunity and generates regulatory T cell precursors. *Nat Immunol*
885 17:304-314.
886 Katz, J.D., B. Wang, K. Haskins, C. Benoist, and D. Mathis. 1993. Following a diabetogenic T cell from genesis
887 through pathogenesis. *Cell* 74:1089-1100.
888 Kawakami, N., F. Odoardi, T. Ziemssen, M. Bradl, T. Ritter, O. Neuhaus, H. Lassmann, H. Wekerle, and A. Flugel.
889 2005. Autoimmune CD4+ T cell memory: lifelong persistence of encephalitogenic T cell clones in
890 healthy immune repertoires. *J Immunol* 175:69-81.
891 Kearney, E.R., K.A. Pape, D.Y. Loh, and M.K. Jenkins. 1994. Visualization of peptide-specific T cell immunity and
892 peripheral tolerance induction in vivo. *Immunity* 1:327-339.
893 Kiesler, P., A. Shakya, D. Tantin, and D. Vercelli. 2009. An allergy-associated polymorphism in a novel regulatory
894 element enhances IL13 expression. *Hum Mol Genet* 18:4513-4520.
895 Kim, H., L. Dickey, C. Stone, J.L. Jafek, T.E. Lane, and D. Tantin. 2019. T cell-selective deletion of Oct1 protects
896 animals from autoimmune neuroinflammation while maintaining neurotropic pathogen response. *J*
897 *Neuroinflammation* 16:133.
898 Kim, U., X.F. Qin, S. Gong, S. Stevens, Y. Luo, M. Nussenzweig, and R.G. Roeder. 1996. The B-cell-specific
899 transcription coactivator OCA-B/OBF-1/Bob-1 is essential for normal production of immunoglobulin
900 isotypes. *Nature* 383:542-547.
901 Klemm, J.D., M.A. Rould, R. Aurora, W. Herr, and C.O. Pabo. 1994. Crystal structure of the Oct-1 POU domain
902 bound to an octamer site: DNA recognition with tethered DNA-binding modules. *Cell* 77:21-32.

903 Krautwald, S., E. Ziegler, K. Tiede, R. Pust, and U. Kunzendorf. 2004. Transduction of the TAT-FLIP fusion
904 protein results in transient resistance to Fas-induced apoptosis in vivo. *The Journal of biological*
905 *chemistry* 279:44005-44011.
906 Krishnamurthy, B., L. Mariana, S.A. Gellert, P.G. Colman, L.C. Harrison, A.M. Lew, P. Santamaria, H.E. Thomas,
907 and T.W. Kay. 2008. Autoimmunity to both proinsulin and IGRP is required for diabetes in nonobese
908 diabetic 8.3 TCR transgenic mice. *J Immunol* 180:4458-4464.
909 Kurts, C., F.R. Carbone, M. Barnden, E. Blanas, J. Allison, W.R. Heath, and J.F. Miller. 1997. CD4+ T cell help
910 impairs CD8+ T cell deletion induced by cross-presentation of self-antigens and favors autoimmunity. *J*
911 *Exp Med* 186:2057-2062.
912 Kurts, C., W.R. Heath, F.R. Carbone, J. Allison, J.F. Miller, and H. Kosaka. 1996. Constitutive class I-restricted
913 exogenous presentation of self antigens in vivo. *J Exp Med* 184:923-930.
914 Leon Rodriguez, D.A., F.D. Carmona, L.E. Echeverria, C.I. Gonzalez, and J. Martin. 2016. IL18 Gene Variants
915 Influence the Susceptibility to Chagas Disease. *PLoS Negl Trop Dis* 10:e0004583.
916 Lernmark, A., and H.E. Larsson. 2013. Immune therapy in type 1 diabetes mellitus. *Nat Rev Endocrinol* 9:92-
917 103.
918 Li, L., Q. He, A. Garland, Z. Yi, L.T. Aybar, T.B. Kepler, J.A. Frelinger, B. Wang, and R. Tisch. 2009. beta cell-
919 specific CD4+ T cell clonotypes in peripheral blood and the pancreatic islets are distinct. *J Immunol*
920 183:7585-7591.
921 Makino, S., Y. Muraoka, Y. Kishimoto, and Y. Hayashi. 1985. Genetic analysis for insulitis in NOD mice. *Jikken*
922 *Dobutsu* 34:425-431.
923 Martinez, R.J., N. Zhang, S.R. Thomas, S.L. Nandiwada, M.K. Jenkins, B.A. Binstadt, and D.L. Mueller. 2012.
924 Arthritogenic self-reactive CD4+ T cells acquire an FR4hiCD73hi anergic state in the presence of Foxp3+
925 regulatory T cells. *J Immunol* 188:170-181.
926 Maurano, M.T., R. Humbert, E. Rynes, R.E. Thurman, E. Haugen, H. Wang, A.P. Reynolds, R. Sandstrom, H. Qu,
927 J. Brody, A. Shafer, F. Neri, K. Lee, T. Kutyavin, S. Stehling-Sun, A.K. Johnson, T.K. Canfield, E. Giste, M.
928 Diegel, D. Bates, R.S. Hansen, S. Neph, P.J. Sabo, S. Heimfeld, A. Raubitschek, S. Ziegler, C. Cotsapas, N.
929 Sotoodehnia, I. Glass, S.R. Sunyaev, R. Kaul, and J.A. Stamatoyannopoulos. 2012. Systematic
930 localization of common disease-associated variation in regulatory DNA. *Science* 337:1190-1195.
931 Nakamura, M., N. Nishida, M. Kawashima, Y. Aiba, A. Tanaka, M. Yasunami, H. Nakamura, A. Komori, M.
932 Nakamuta, M. Zeniya, E. Hashimoto, H. Ohira, K. Yamamoto, M. Onji, S. Kaneko, M. Honda, S.
933 Yamagiwa, K. Nakao, T. Ichida, H. Takikawa, M. Seike, T. Umemura, Y. Ueno, S. Sakisaka, K. Kikuchi, H.
934 Ebinuma, N. Yamashiki, S. Tamura, Y. Sugawara, A. Mori, S. Yagi, K. Shirabe, A. Taketomi, K. Arai, K.
935 Monoe, T. Ichikawa, M. Taniai, Y. Miyake, T. Kumagi, M. Abe, K. Yoshizawa, S. Joshita, S. Shimoda, K.
936 Honda, H. Takahashi, K. Hirano, Y. Takeyama, K. Harada, K. Migita, M. Ito, H. Yatsuhashi, N. Fukushima,
937 H. Ota, T. Komatsu, T. Saoshiro, J. Ishida, H. Kouno, H. Kouno, M. Yagura, M. Kobayashi, T. Muro, N.
938 Masaki, K. Hirata, Y. Watanabe, Y. Nakamura, M. Shimada, N. Hirashima, T. Komeda, K. Sugi, M. Koga,
939 K. Ario, E. Takesaki, Y. Maehara, S. Uemoto, N. Kokudo, H. Tsubouchi, M. Mizokami, Y. Nakanuma, K.
940 Tokunaga, and H. Ishibashi. 2012. Genome-wide association study identifies TNFSF15 and POU2AF1 as
941 susceptibility loci for primary biliary cirrhosis in the Japanese population. *Am J Hum Genet* 91:721-728.
942 Newby, B.N., T.M. Brusko, B. Zou, M.A. Atkinson, M. Clare-Salzler, and C.E. Mathews. 2017. Type 1 Interferons
943 Potentiate Human CD8(+) T-Cell Cytotoxicity Through a STAT4- and Granzyme B-Dependent Pathway.
944 *Diabetes* 66:3061-3071.
945 Parker, M.J., S. Xue, J.J. Alexander, C.H. Wasserfall, M.L. Campbell-Thompson, M. Battaglia, S. Gregori, C.E.
946 Mathews, S. Song, M. Troutt, S. Eisenbeis, J. Williams, D.A. Schatz, M.J. Haller, and M.A. Atkinson.
947 2009. Immune depletion with cellular mobilization imparts immunoregulation and reverses
948 autoimmune diabetes in nonobese diabetic mice. *Diabetes* 58:2277-2284.
949 Peterson, J.D., R. Berg, J.D. Piganelli, M. Poulin, and K. Haskins. 1998. Analysis of leukocytes recruited to the
950 pancreas by diabetogenic T cell clones. *Cell Immunol* 189:92-98.

951 Polo, J.M., T. Dell'Oso, S.M. Ranuncolo, L. Cerchietti, D. Beck, G.F. Da Silva, G.G. Prive, J.D. Licht, and A.
952 Melnick. 2004. Specific peptide interference reveals BCL6 transcriptional and oncogenic mechanisms in
953 B-cell lymphoma cells. *Nat Med* 10:1329-1335.
954 Presa, M., Y.G. Chen, A.E. Grier, E.H. Leiter, M.A. Brehm, D.L. Greiner, L.D. Shultz, and D.V. Serreze. 2015. The
955 Presence and Preferential Activation of Regulatory T Cells Diminish Adoptive Transfer of Autoimmune
956 Diabetes by Polyclonal Nonobese Diabetic (NOD) T Cell Effectors into NSG versus NOD-scid Mice. *J*
957 *Immunol* 195:3011-3019.
958 Qin, X.F., A. Reichlin, Y. Luo, R.G. Roeder, and M.C. Nussenzweig. 1998. OCA-B integrates B cell antigen
959 receptor-, CD40L- and IL 4-mediated signals for the germinal center pathway of B cell development.
960 *EMBO J* 17:5066-5075.
961 Rosmalen, J.G., T. Martin, C. Dobbs, J.S. Voerman, H.A. Drexhage, K. Haskins, and P.J. Leenen. 2000. Subsets of
962 macrophages and dendritic cells in nonobese diabetic mouse pancreatic inflammatory infiltrates:
963 correlation with the development of diabetes. *Lab Invest* 80:23-30.
964 Schloot, N.C., P. Hanifi-Moghaddam, C. Goebel, S.V. Shatavi, S. Flohe, H. Kolb, and H. Rothe. 2002. Serum IFN-
965 gamma and IL-10 levels are associated with disease progression in non-obese diabetic mice. *Diabetes*
966 *Metab Res Rev* 18:64-70.
967 Schwarze, S.R., K.A. Hruska, and S.F. Dowdy. 2000. Protein transduction: unrestricted delivery into all cells?
968 *Trends Cell Biol* 10:290-295.
969 Serreze, D.V., M. Bridgett, H.D. Chapman, E. Chen, S.D. Richard, and E.H. Leiter. 1998. Subcongenic analysis of
970 the Idd13 locus in NOD/Lt mice: evidence for several susceptibility genes including a possible
971 diabetogenic role for beta 2-microglobulin. *J Immunol* 160:1472-1478.
972 Serreze, D.V., H.D. Chapman, D.S. Varnum, M.S. Hanson, P.C. Reifsnyder, S.D. Richard, S.A. Fleming, E.H. Leiter,
973 and L.D. Shultz. 1996. B lymphocytes are essential for the initiation of T cell-mediated autoimmune
974 diabetes: analysis of a new "speed congenic" stock of NOD.Ig mu null mice. *J Exp Med* 184:2049-2053.
975 Shakya, A., A. Goren, A. Shalek, C.N. German, J. Snook, V.K. Kuchroo, N. Yosef, R.C. Chan, A. Regev, M.A.
976 Williams, and D. Tantin. 2015. Oct1 and OCA-B are selectively required for CD4 memory T cell function.
977 *J Exp Med* 212:2115-2131.
978 Shakya, A., J. Kang, J. Chumley, M.A. Williams, and D. Tantin. 2011. Oct1 is a switchable, bipotential stabilizer
979 of repressed and inducible transcriptional states. *The Journal of biological chemistry* 286:450-459.
980 Shi, W., Y. Liao, S.N. Willis, N. Taubenheim, M. Inouye, D.M. Tarlinton, G.K. Smyth, P.D. Hodgkin, S.L. Nutt, and
981 L.M. Corcoran. 2015. Transcriptional profiling of mouse B cell terminal differentiation defines a
982 signature for antibody-secreting plasma cells. *Nat Immunol* 16:663-673.
983 Sitrin, J., A. Ring, K.C. Garcia, C. Benoist, and D. Mathis. 2013. Regulatory T cells control NK cells in an insulitic
984 lesion by depriving them of IL-2. *J Exp Med* 210:1153-1165.
985 Skwarczynska, M., and C. Ottmann. 2015. Protein-protein interactions as drug targets. *Future Med Chem*
986 7:2195-2219.
987 Staeva, T.P., L. Chatenoud, R. Insel, and M.A. Atkinson. 2013. Recent lessons learned from prevention and
988 recent-onset type 1 diabetes immunotherapy trials. *Diabetes* 62:9-17.
989 Sun, J., G. Matthias, M.J. Mihatsch, K. Georgopoulos, and P. Matthias. 2003. Lack of the transcriptional
990 coactivator OBF-1 prevents the development of systemic lupus erythematosus-like phenotypes in
991 Aiolos mutant mice. *J Immunol* 170:1699-1706.
992 Testa, G., J. Schaft, F. van der Hoeven, S. Glaser, K. Anastassiadis, Y. Zhang, T. Hermann, W. Stremmel, and A.F.
993 Stewart. 2004. A reliable lacZ expression reporter cassette for multipurpose, knockout-first alleles.
994 *Genesis* 38:151-158.
995 Thin, T.H., E. Kim, S. Yeh, E.R. Sampson, Y.T. Chen, L.L. Collins, R. Basavappa, and C. Chang. 2002. Mutations in
996 the helix 3 region of the androgen receptor abrogate ARA70 promotion of 17beta-estradiol-induced
997 androgen receptor transactivation. *The Journal of biological chemistry* 277:36499-36508.
998 Tuettenberg, A., E. Huter, M. Hubo, J. Horn, J. Knop, B. Grimbacher, R.A. Kroczek, S. Stoll, and H. Jonuleit. 2009.
999 The role of ICOS in directing T cell responses: ICOS-dependent induction of T cell anergy by tolerogenic
1000 dendritic cells. *J Immunol* 182:3349-3356.

1001 Van Belle, T.L., P. Taylor, and M.G. von Herrath. 2009. Mouse Models for Type 1 Diabetes. *Drug Discov Today*
1002 *Dis Models* 6:41-45.
1003 van Heel, D.A., I.A. Udalova, A.P. De Silva, D.P. McGovern, Y. Kinouchi, J. Hull, N.J. Lench, L.R. Cardon, A.H.
1004 Carey, D.P. Jewell, and D. Kwiatkowski. 2002. Inflammatory bowel disease is associated with a TNF
1005 polymorphism that affects an interaction between the OCT1 and NF(-kappa)B transcription factors.
1006 *Hum Mol Genet* 11:1281-1289.
1007 Vanasek, T.L., A. Khoruts, T. Zell, and D.L. Mueller. 2001. Antagonistic roles for CTLA-4 and the mammalian
1008 target of rapamycin in the regulation of clonal anergy: enhanced cell cycle progression promotes recall
1009 antigen responsiveness. *J Immunol* 167:5636-5644.
1010 Verdaguer, J., D. Schmidt, A. Amrani, B. Anderson, N. Averill, and P. Santamaria. 1997. Spontaneous
1011 autoimmune diabetes in monoclonal T cell nonobese diabetic mice. *J Exp Med* 186:1663-1676.
1012 Vince, N., H. Li, V. Ramsuran, V. Naranbhai, F.M. Duh, B.P. Fairfax, B. Saleh, J.C. Knight, S.K. Anderson, and M.
1013 Carrington. 2016. HLA-C Level Is Regulated by a Polymorphic Oct1 Binding Site in the HLA-C Promoter
1014 Region. *Am J Hum Genet* 99:1353-1358.
1015 Wang, B., I. Andre, A. Gonzalez, J.D. Katz, M. Aguet, C. Benoist, and D. Mathis. 1997. Interferon-gamma
1016 impacts at multiple points during the progression of autoimmune diabetes. *Proc Natl Acad Sci U S A*
1017 94:13844-13849.
1018 Wong, C.P., L. Li, J.A. Frelinger, and R. Tisch. 2006. Early autoimmune destruction of islet grafts is associated
1019 with a restricted repertoire of IGRP-specific CD8+ T cells in diabetic nonobese diabetic mice. *J Immunol*
1020 176:1637-1644.
1021 Yamane, K., C. Toumazou, Y. Tsukada, H. Erdjument-Bromage, P. Tempst, J. Wong, and Y. Zhang. 2006.
1022 JHDM2A, a JmjC-containing H3K9 demethylase, facilitates transcription activation by androgen
1023 receptor. *Cell* 125:483-495.
1024 Yeo, L., A. Woodwyk, S. Sood, A. Lorenc, M. Eichmann, I. Pujol-Autonell, R. Melchiotti, A. Skowera, E. Fidanis,
1025 G.M. Dolton, K. Tungatt, A.K. Sewell, S. Heck, A. Saxena, C.A. Beam, and M. Peakman. 2018.
1026 Autoreactive T effector memory differentiation mirrors beta cell function in type 1 diabetes. *J Clin*
1027 *Invest* 128:3460-3474.
1028 Yosef, N., A.K. Shalek, J.T. Gaublomme, H. Jin, Y. Lee, A. Awasthi, C. Wu, K. Karwacz, S. Xiao, M. Jorgolli, D.
1029 Gennert, R. Satija, A. Shakya, D.Y. Lu, J.J. Trombetta, M.R. Pillai, P.J. Ratcliffe, M.L. Coleman, M. Bix, D.
1030 Tantin, H. Park, V.K. Kuchroo, and A. Regev. 2013. Dynamic regulatory network controlling TH17 cell
1031 differentiation. *Nature* 496:461-468.
1032 Zhang, C., I. Todorov, C.L. Lin, M. Atkinson, F. Kandeel, S. Forman, and D. Zeng. 2007. Elimination of insulitis
1033 and augmentation of islet beta cell regeneration via induction of chimerism in overtly diabetic NOD
1034 mice. *Proc Natl Acad Sci U S A* 104:2337-2342.
1035 Zuber, J., J. Shi, E. Wang, A.R. Rappaport, H. Herrmann, E.A. Sison, D. Magoon, J. Qi, K. Blatt, M. Wunderlich,
1036 M.J. Taylor, C. Johns, A. Chicas, J.C. Mulloy, S.C. Kogan, P. Brown, P. Valent, J.E. Bradner, S.W. Lowe,
1037 and C.R. Vakoc. 2011. RNAi screen identifies Brd4 as a therapeutic target in acute myeloid leukaemia.
1038 *Nature* 478:524-528.
1039 Zwilling, S., A. Dieckmann, P. Pfisterer, P. Angel, and T. Wirth. 1997. Inducible expression and phosphorylation
1040 of coactivator BOB.1/OBF.1 in T cells. *Science* 277:221-225.

1041

Kim et al. Figure 1

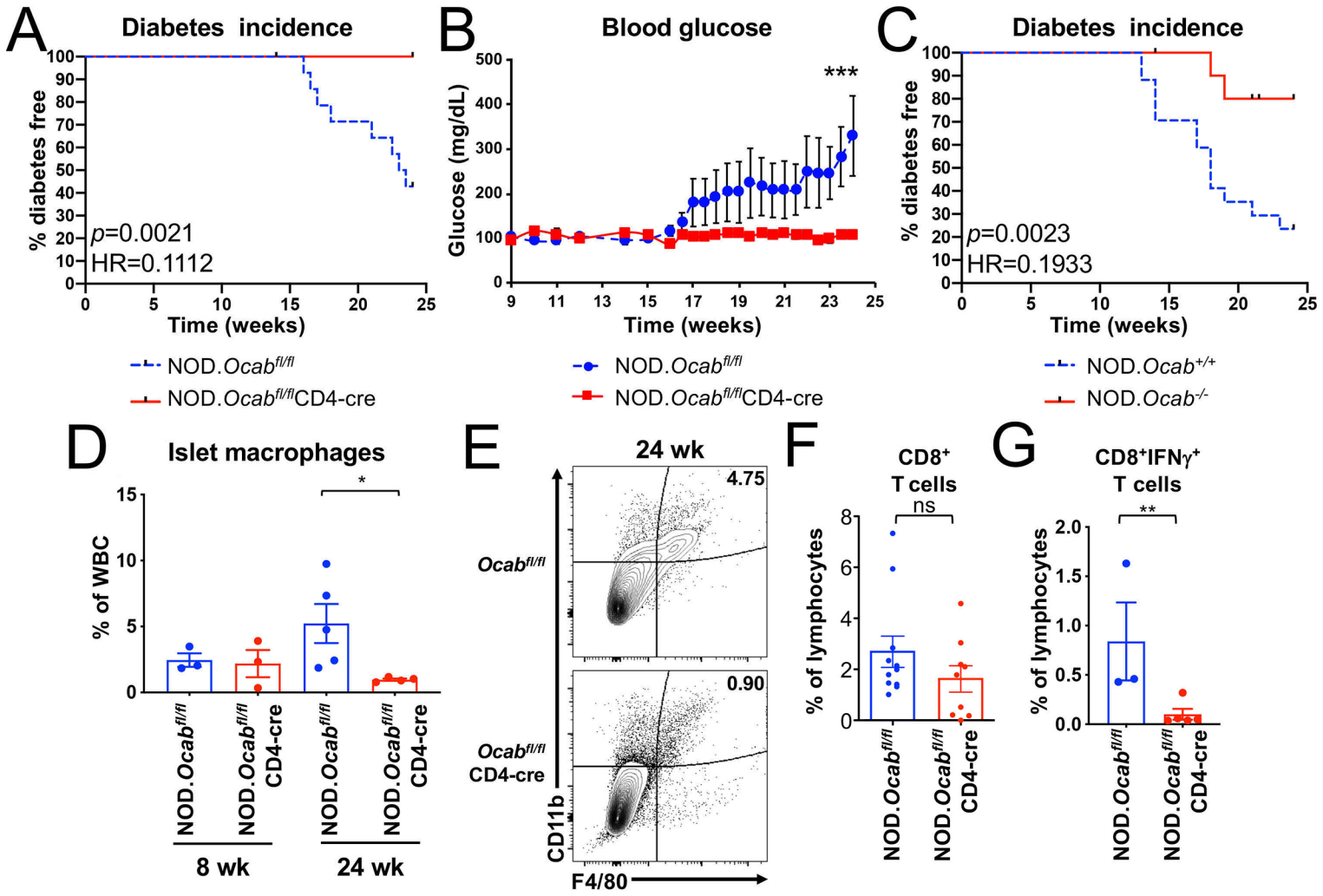

Kim et al. Figure 2

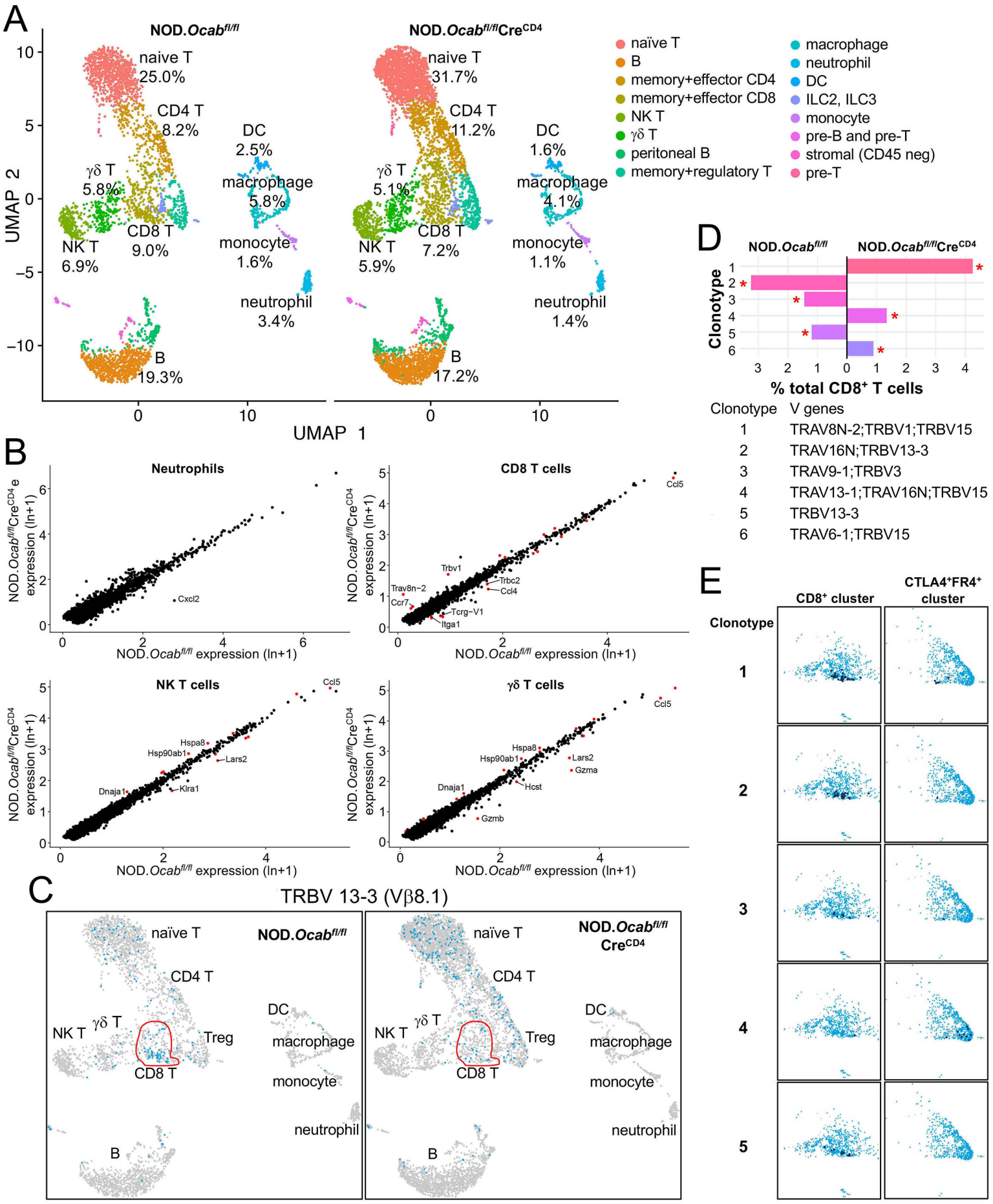

Clonotype	V genes
1	TRAV8N-2;TRBV1;TRBV15
2	TRAV16N;TRBV13-3
3	TRAV9-1;TRBV3
4	TRAV13-1;TRAV16N;TRBV15
5	TRBV13-3
6	TRAV6-1;TRBV15

Kim et al. Figure 3

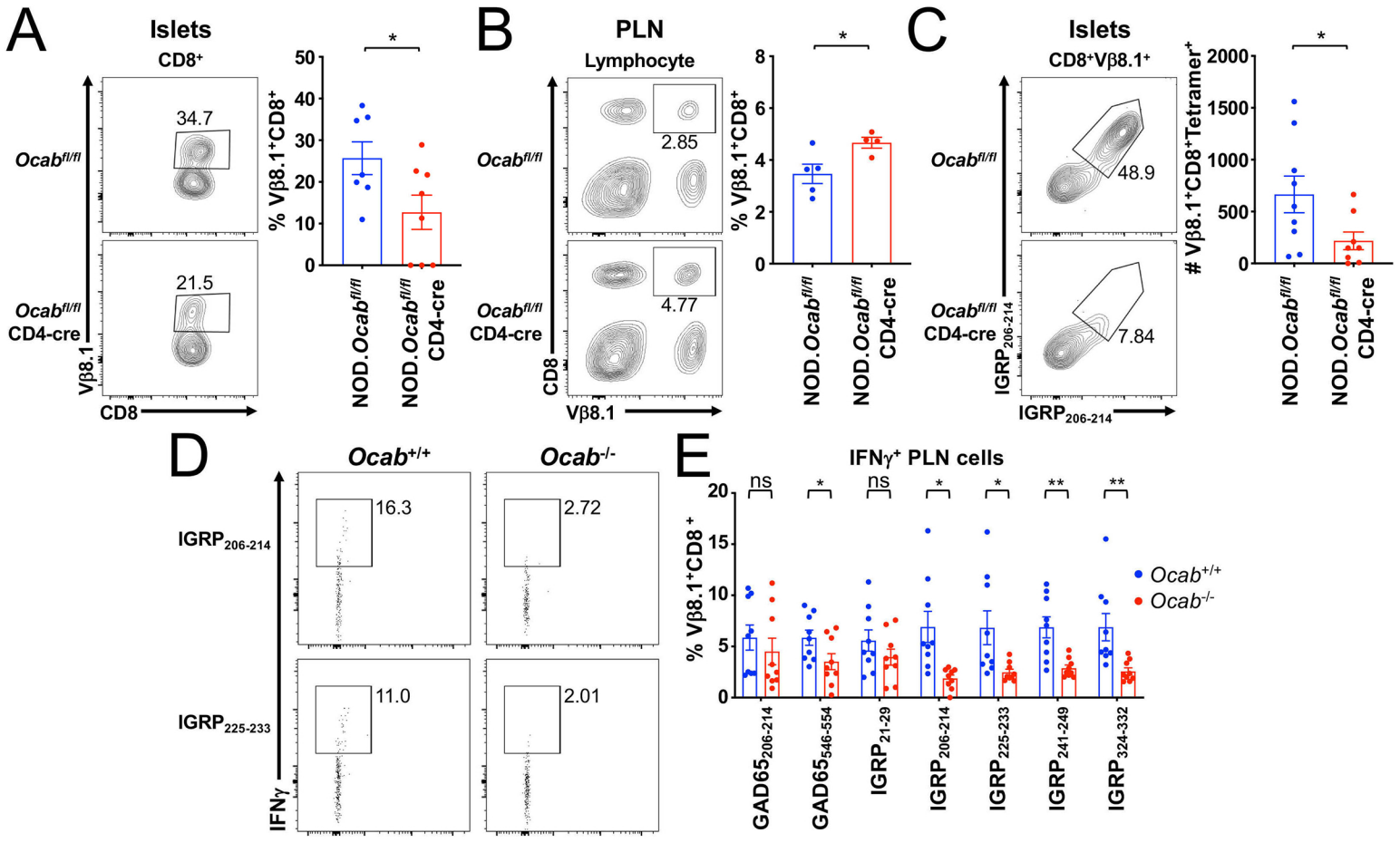

Kim et al. Figure 4

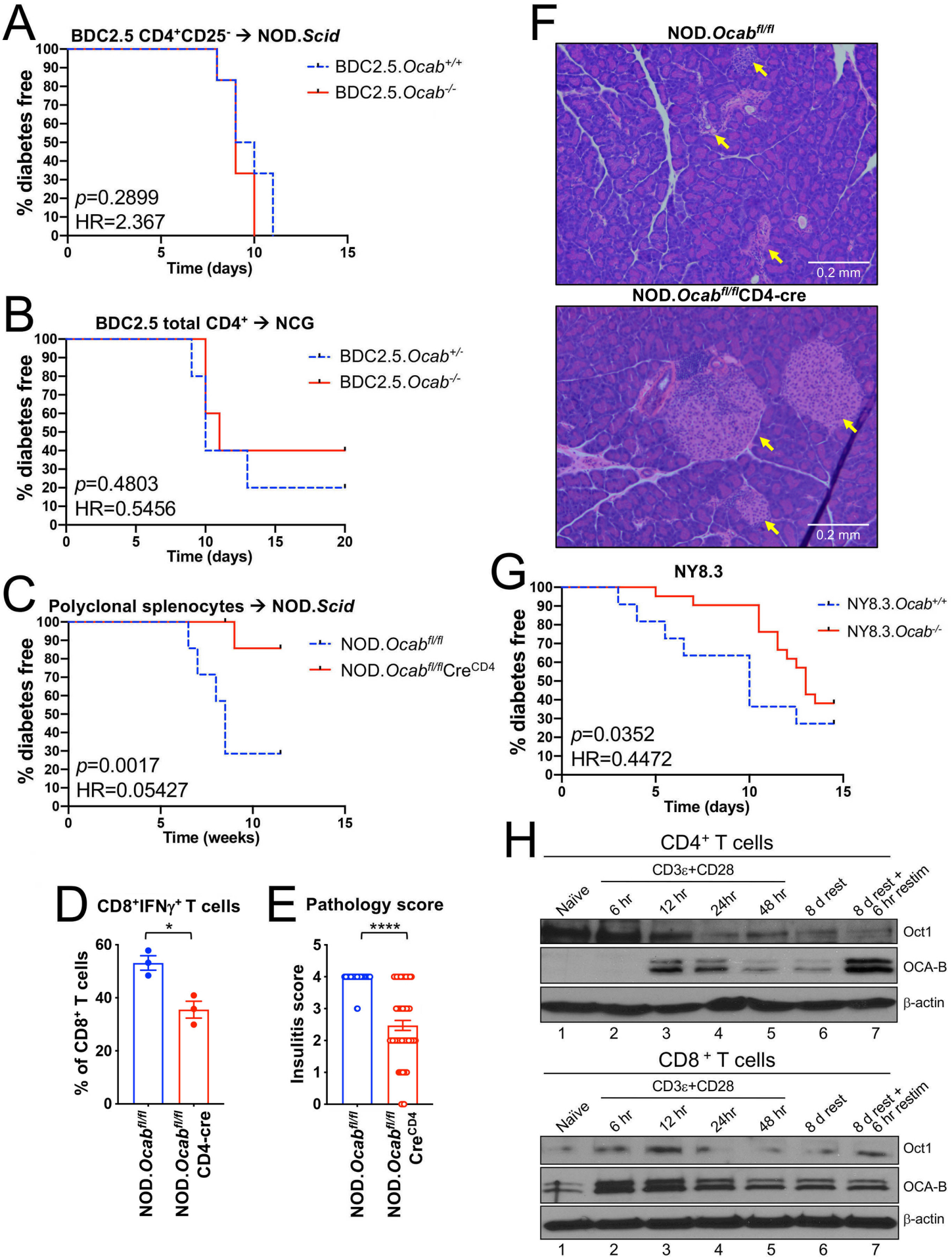

Kim et al. Figure 5

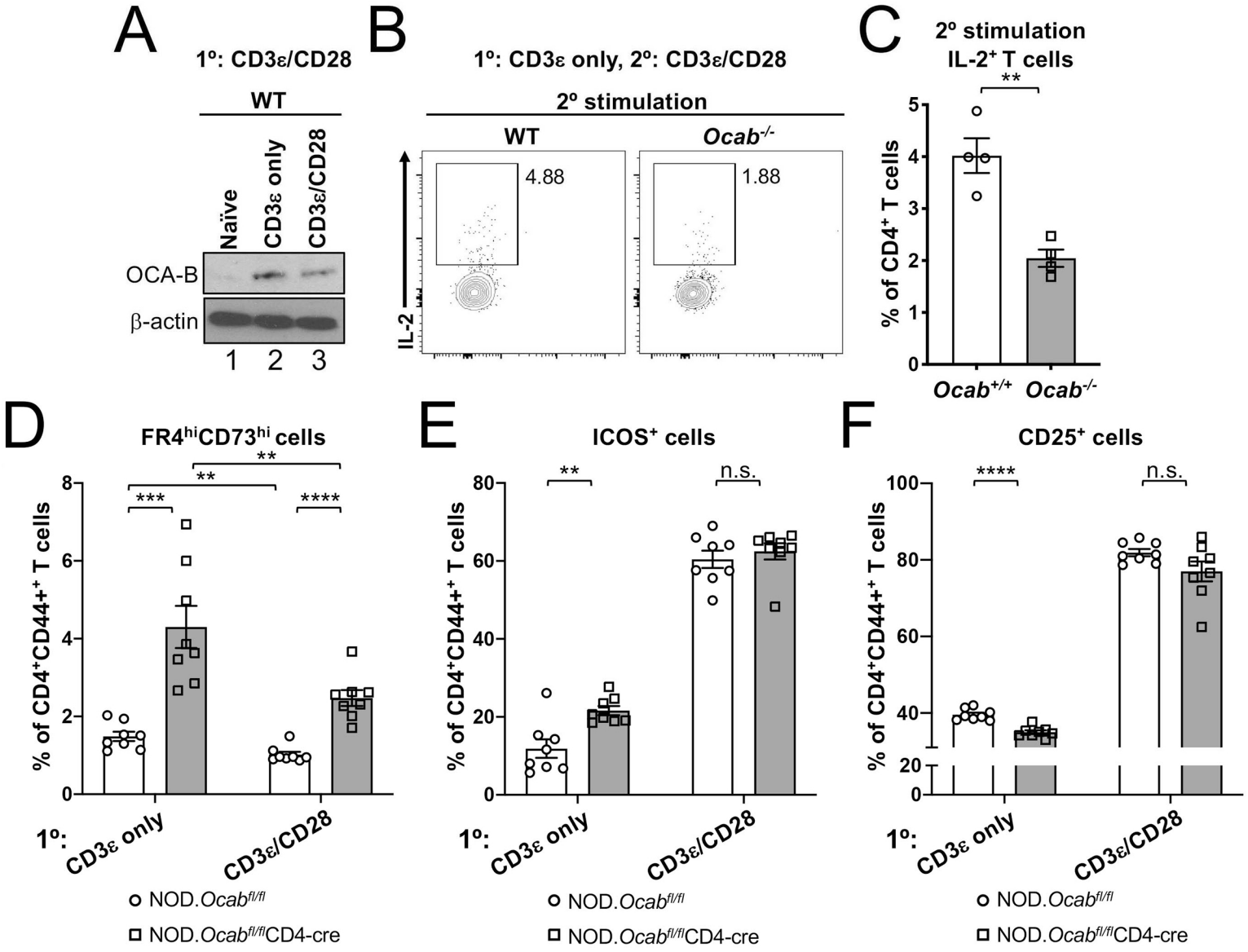

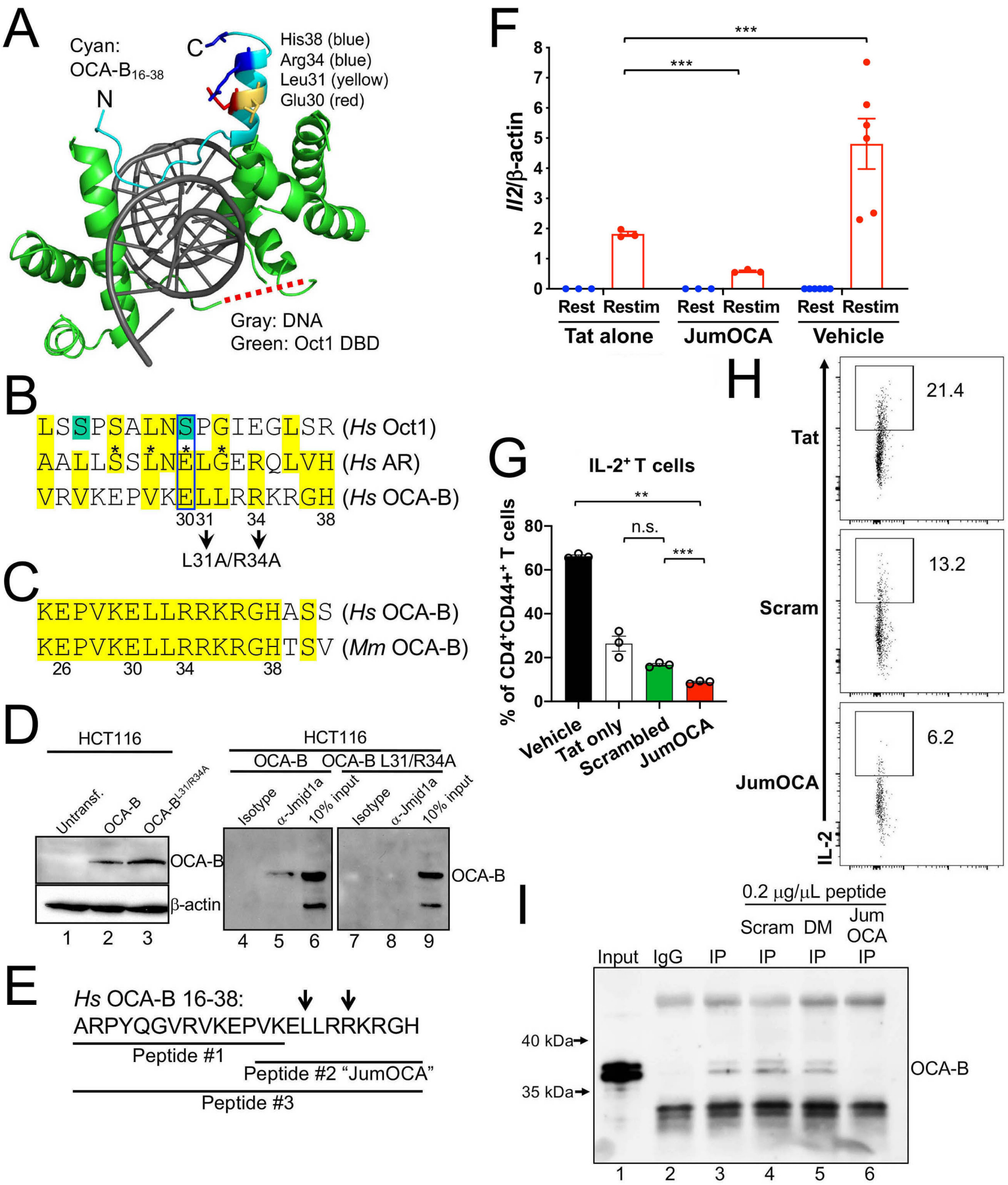
A
Cyan:
OCA-B16-38
N
C
His38 (blue)
Arg34 (blue)
Leu31 (yellow)
Glu30 (red)
Gray: DNA
Green: Oct1 DBD
B
LSSPSALNSPGIEGLSR (Hs Oct1)
AALLSSLNELGERQLVH (Hs AR)
VRVKEPVKELLRRKRGH (Hs OCA-B)
30 31 34 38
L31A/R34A
C
KEPVKELLRRKRGHASS (Hs OCA-B)
KEPVKELLRRKRGHTSV (Mm OCA-B)
26 30 34 38
D
HCT116
Untransf.
OCA-B
OCA-BL31/R34A
OCA-B
β-actin
1 2 3
HCT116
OCA-B OCA-B L31/R34A
Isotype
α-Jmjd1a
10% input
OCA-B
4 5 6 7 8 9
E
Hs OCA-B 16-38:
ARPYQGVRVKEPVKELLRRKRGH
Peptide #1
Peptide #2 "JumOCA"
Peptide #3
F
Il2/β-actin
Rest Restim Rest Restim Rest Restim
Tat alone
JumOCA
Vehicle
G
IL-2+ T cells
% of CD4+CD44+ T cells
Vehicle
Tat only
Scrambled
JumOCA
H
Tat
Scram
JumOCA
IL-2
21.4
13.2
6.2
I
0.2 μg/μL peptide
Scram DM Jum OCA
Input IgG IP IP IP IP
40 kDa
35 kDa
OCA-B
1 2 3 4 5 6
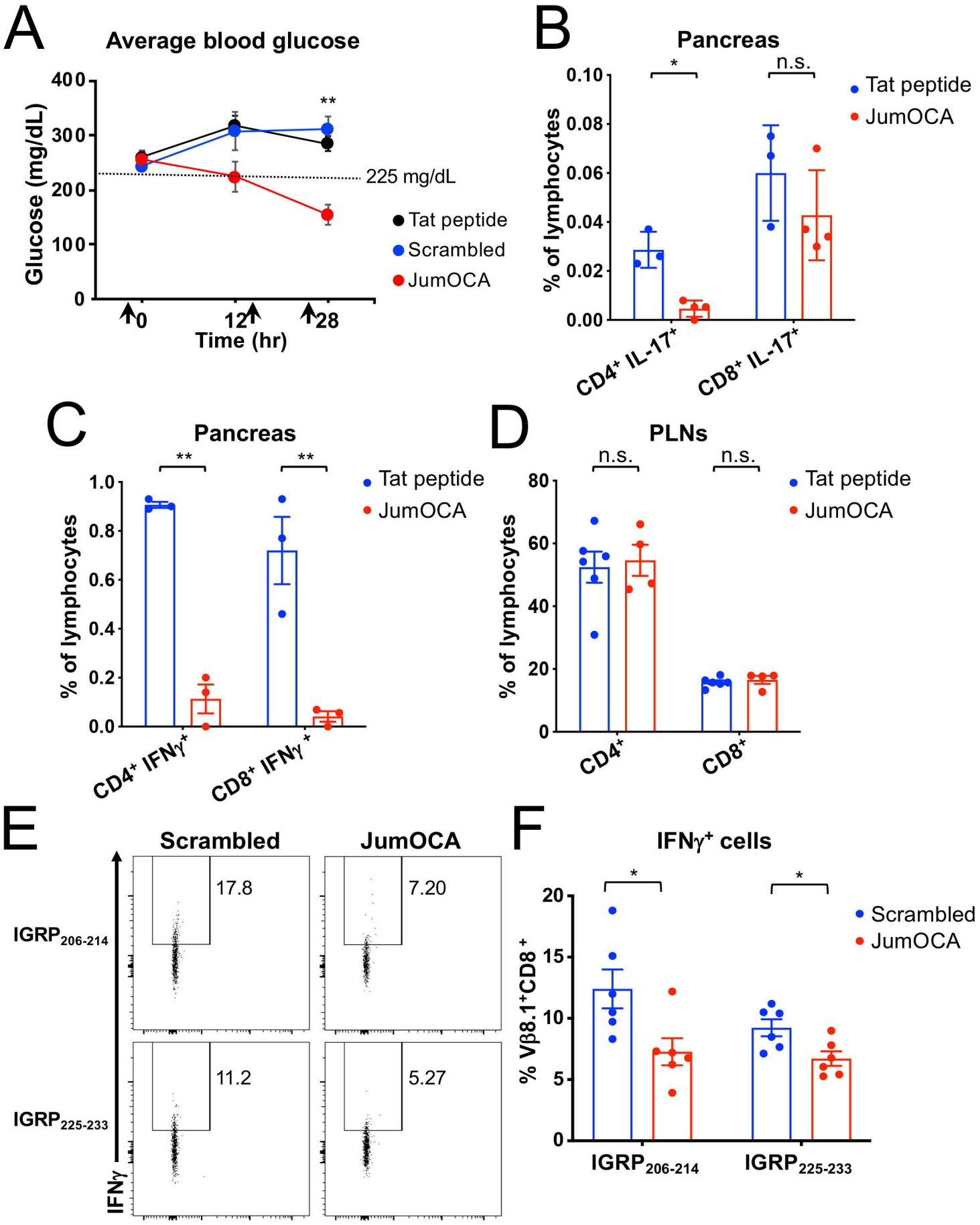
Kim et al. Figure 7